

March 2018

# Modeling Corrosion Damage and Repair to a 3

Joseph R. Scott

*University of South Florida*, [josephscott@mail.usf.edu](mailto:josephscott@mail.usf.edu)

Follow this and additional works at: <http://scholarcommons.usf.edu/etd>

 Part of the [Civil Engineering Commons](#)

---

## Scholar Commons Citation

Scott, Joseph R., "Modeling Corrosion Damage and Repair to a 3" (2018). *Graduate Theses and Dissertations*.  
<http://scholarcommons.usf.edu/etd/7228>

This Thesis is brought to you for free and open access by the Graduate School at Scholar Commons. It has been accepted for inclusion in Graduate Theses and Dissertations by an authorized administrator of Scholar Commons. For more information, please contact [scholarcommons@usf.edu](mailto:scholarcommons@usf.edu).

Modeling Corrosion Damage and Repair to a 3<sup>rd</sup> Scale Concrete Bridge Bent

by

Joseph R. Scott

A thesis submitted in partial fulfillment  
of the requirements for the degree of  
Master of Science in Civil Engineering  
Department of Civil and Environmental Engineering  
College of Engineering  
University of South Florida

Major Professor: A. Gray Mullins, Ph.D.  
Rajan Sen, Ph.D.  
Michael J. Stokes, Ph.D.

Date of Approval:  
March 7, 2018

Keywords: Deficiencies, Carbon Fiber Reinforcing Polymer, Prestress  
Transfer Length, Area Loss of Steel, Lateral Deflection

Copyright © 2018, Joseph R. Scott

## **DEDICATION**

To David Vincent.

## **ACKNOWLEDGMENTS**

I am sincerely grateful of my experience in research engineering owed to Dr. Mullins, Dr. Sen, Dr. Stokes and Dr. Sagüés, who have guided and equipped me with conceptual and practical tools in skillful problem solving and logical development of scientific experimentation. Their unsurpassed ability and dedication to facilitate learning in both classrooms and field environments delivers a highly valued learning experience, which has undoubtedly broadened and positively shaped my understanding of the engineering profession.

I am thankful for the opportunity to work with a dedicated, well distinguished, cohesive team of bright minded individuals within the University of South Florida's Structural/Geotechnical engineering research group.

A special thanks to Michelle Nobel and Tom Zuppa from Sika Corporation, for donating material and providing technical guidance that led toward success of this experiment.



## TABLE OF CONTENTS

LIST OF TABLES	iii
LIST OF FIGURES	iv
ABSTRACT	vii
CHAPTER 1: INTRODUCTION	1
1.1 Problem Statement	1
1.2 Organization of Thesis	3
CHAPTER 2: BACKGROUND	4
2.1 Corrosion	4
2.2 Corrosion Initiation	5
2.3 Corrosion Damage of Bridges	6
2.4 Rehabilitation Alternatives	7
2.5 Pilot Study	9
2.6 Scope of Study	16
CHAPTER 3: MODELING CORROSION DAMAGED PILE BENTS	18
3.1 FLPIER	18
3.2 Model Assumptions	19
3.3 Influencing Variables and Input Parameters	20
3.4 Modulus of Elasticity of Concrete	21
3.5 Prestress Transfer Length	24
3.6 Undamaged Control Model	26
3.7 Damaged Models	32
CHAPTER 4: MODELING FRP-REPAIRED PILE BENTS	40
4.1 CFRP Tensile Design Calculation	41
4.2 Repair Models and Carbon Shell Distribution	41
CHAPTER 5: CONCLUSIONS	47
5.1 Study Summary	47
5.2 Interpretations of Findings	49
5.3 Future Work	49
REFERENCES	50
APPENDIX A: PILE DEFICIENCY MAPPING	52



## LIST OF TABLES

Table 2.1 Calculation parameters.	6
Table 2.2 Max load and displacement response with respect to increasing damage level.	14
Table 2.3 Undamaged bent measured loss in capacity due to loss in steel area.	15
Table 3.1 Model input parameters.	20
Table 3.2 Percent area loss with respect to effective area of steel.	24
Table 3.3 Percent area loss with respect to loss in steel prestress.	24
Table 3.4 Diameter of stand multiplication factors.	25
Table 3.5 Results of damages to models pile bents at max lateral load.	38
Table 4.1 Model results for single ply CFRP repair with respect to damage.	43

## LIST OF FIGURES

Figure 1.1 Pile bent from 1950s era Gandy Bridge, Tampa Bay, Florida.	1
Figure 1.2 Cap and column configuration - Gandy Bridge adjacent to the navigation channel.	2
Figure 1.3 Corroding steel in one bent pile in east bound Gandy Bridge (built circa 1970).	3
Figure 2.1 Pourbaix diagram for iron (ACI 222R-89).	6
Figure 2.2 Pre-repair removal of chloride contaminated concrete.	8
Figure 2.3 Corrosion cells instrumented on piles.	10
Figure 2.4 Inflection points of Florida bridges and modeled bridge (Goulish, 2002).	12
Figure 2.5 Testing instrumentation on pile bent (Goulish, 2002).	12
Figure 2.6 Lateral load vs lateral displacement at pile cap (Goulish 2002).	14
Figure 2.7 50% damage bent prior to testing.	15
Figure 2.8 Existing pile identification.	17
Figure 2.9 Elevation view of bent.	17
Figure 2.10 Pile and cap reinforcing scheme.	17
Figure 3.1 FLPIER nodes.	21
Figure 3.2 Modeling undamaged bent varying concrete modulus.	22
Figure 3.3 Stress/Force change with respect to area of prestressing steel.	23
Figure 3.4 Control model segments elevation view (ft).	27
Figure 3.5 Geotechnical characteristics of FLPIER model (ft).	27
Figure 3.6 Measured vs undamaged model load-displacement curve.	28
Figure 3.7 Pile count and coordinate orientation.	29

Figure 3.8 Undamaged model with sustained service loads and at ultimate lateral load.	29
Figure 3.9 Undamaged model max shear.	30
Figure 3.10 Undamaged model max moment.	30
Figure 3.11 Undamaged model max displacement.	31
Figure 3.12 Interaction diagram for load case 10.	31
Figure 3.13 Response curves for all models.	32
Figure 3.14 Interaction envelope for all models.	33
Figure 3.15 90% damaged pile count.	34
Figure 3.16 90% damaged model sustained service loads and ultimate lateral load.	34
Figure 3.17 90% damaged model max shear.	35
Figure 3.18 90% damaged model max moment.	35
Figure 3.19 90% damaged model max axial force.	36
Figure 3.20 90% damaged model max displacement.	36
Figure 3.21 Interaction diagram 90% damaged model at load case 10.	37
Figure 3.22 Maximum applied lateral load with respect to loss in steel area.	38
Figure 3.23 Maximum moment in bent with respect to loss in steel area.	38
Figure 3.24 Maximum shear in bent with respect to loss in steel area.	39
Figure 3.25 Maximum lateral displacement in bent with respect to loss in steel area.	39
Figure 4.1 CFRP design schematic.	40
Figure 4.2 Strength requirements for repair material.	41
Figure 4.3 Square cross section with custom reinforcement.	42
Figure 4.4 90% Single ply repaired damage at maximum load case.	43
Figure 4.5 90% single ply repaired damage at maximum load case.	44

Figure 4.6 90% single ply repaired damage shear at maximum load case.	44
Figure 4.7 90% single ply repaired damage moment at maximum load case.	45
Figure 4.8 90% single ply repaired damage axial at maximum lateral loading.	45
Figure 4.9 90% single ply repaired damage displacement at maximum load case.	46
Figure 4.10 Interaction diagram single ply damage repaired at load case 10.	46
Figure 5.1 Response of measured, modeled and repaired at 50% damage.	47
Figure 5.2 Measured damage vs single ply repair modeled damage at 90%.	48
Figure 5.3 Interaction diagram of control model and repaired damage.	48
Figure A.1 Pile S223 deficiency map.	53
Figure A.2 Pile S222 deficiency map.	54
Figure A.3 Pile S221 deficiency map.	55
Figure A.4 S220 deficiency map.	56
Figure A.5 S218 deficiency map.	57
Figure B.1 Measured test data from undamaged pile bent.	59
Figure B.2 Undamaged model, undamaged measured model, undamaged repaired model.	59
Figure B.3 10% Damage model, 10% measured damage, 10% repaired damage.	60
Figure B.4 30% Damage model, 30% measured damage, 30% repaired damage.	60
Figure B.5 50% Damage model, 50% measured damage, 50% repaired damage.	61
Figure B.6 All damaged models.	61
Figure B.7 Interaction diagram of all damaged models.	62
Figure B.8 Lateral load response for all repaired damage models.	62
Figure B.9 Interaction diagram envelope for all repaired damage models.	63

## ABSTRACT

The main purpose of this study was to investigate and implement a repair design for corrosion damaged bridge bents in order to resist lateral loading, such as wind loads or ship impact. Using the results from a one-third scale bridge bent constructed and tested for a previous study, non-linear modeling was used to simulate the same corrosion damage and load response. The principle variable considered was damage, represented as a percent of effective area loss of prestressing steel within a designated damage zone along the length of piles. Other influencing variables included: prestress transfer length, localized loss in prestress due to corrosion damage, prestress force, and concrete modulus of elasticity.

Upon successful convergence of measured and modeled results, carbon fiber repair schemes were then modeled to restore bents to their full capacity. Suitable repairs were judged on the basis of restoration of capacity of the entire pile bent and the interaction diagrams of the individual piles. Results of the modeled repairs suggested that a single layer of a commercially available unidirectional carbon fiber would be sufficient when aligned longitudinally. No benefit from accompanying transverse fibers were considered although such a repair was suggested by the study findings.

Analysis indicated that longitudinally bonded carbon fiber reinforced polymer (CFRP) to bridge piles increases a bent's ability to resist bending moment due to lateral loading at the cap. However, additional capacity to plastic region of the response curve indicated larger capacity gains than by gains to elastic regions.

## CHAPTER 1: INTRODUCTION

### 1.1 Problem Statement

Many of today's aging overwater bridges were built using pile bents to form the pier foundation support. Figure 1.1 shows a pile bent which is a group of piles (usually driven piles) with a pile cap that also serves as the support for the beams that span from pier to pier. Until the late 1970s and 80s, pile bents were the pier type of choice for lower level bridges due to economy. For higher portions of the bridge that might need to provide vessel clearance, the pile bent configuration becomes too tall and slender to provide the required stability and were often exchanged for a cap and column configuration (Figure 1.2) which is more economical and effective in those situations. Note in Figure 1.2 a water level pile cap (footing) is formed around a group of piles and a larger stronger column then extends up to the base of the bridge.

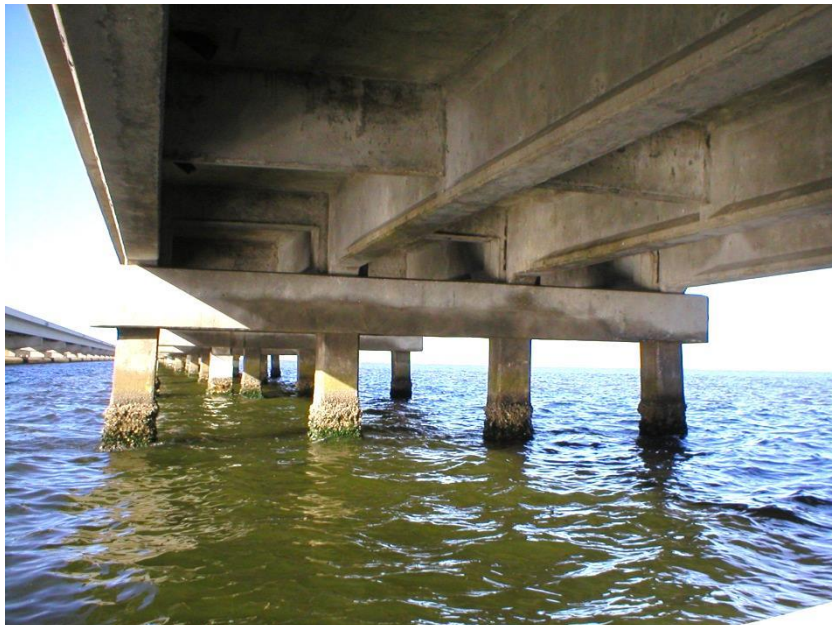


Figure 1.1 Pile bent from 1950s era Gandy Bridge, Tampa Bay, Florida.





Figure 1.2 Cap and column configuration - Gandy Bridge adjacent to the navigation channel.

In later years, cap and column designs with far more piles per footing became more common for all over water bridges with large vessel traffic so that all piles could contribute more effectively in resisting lateral forces associated with vessel collisions. However, pile bents still support a significant portion of intra-coastal waterway crossing bridges over corrosive marine environments.

Aside from the pile driving stresses associated with first installation of the piles, the highest stresses experienced by piles in bents stem from lateral forces from hurricane force winds or vessel collisions. Corrosion of the reinforcing steel in piles results in drastic reductions in bending resistance due to loss of concrete and steel section (Figure 1.3).

This study investigates loss of capacity in bridge pile bents damaged by corrosion. The scope of this study uses non-linear finite element analyses to develop models that both represent multistage damage of pile bents and then models repair schemes with externally applied carbon fiber fabric which can be applied to existing bridges in poor condition.



Figure 1.3 Corroding steel in one bent pile in east bound Gandy Bridge (built circa 1970).

## **1.2 Organization of Thesis**

This thesis is divided into four ensuing chapters which provide an overview of the entire study. Chapter 2 details the process by which corrosion damages reinforced concrete pile bents. Chapter 3 explains the process and outlines assumptions, input parameters and influencing variables required in modeling an undamaged pile bent, damaged bents, and repaired bents. Chapter 4 presents the repair design and details parameters used to model CFRP repaired bents. Chapter 5 provides a summary of findings and outlines future work required to further scientific understanding of damage and repair of damage to aging bridge infrastructure in aggressive marine environments.

## CHAPTER 2: BACKGROUND

### 2.1 Corrosion

Corrosion damage to marine infrastructure accounts for nearly 3.2% of the United States gross domestic product. According to the ASCE 2017 infrastructure report card, America's bridge infrastructure grade is a C+, where 9.1% of the nation's bridges were deemed structurally deficient in 2016. Of the U.S.'s 614,378 bridges, nearly 4 in 10 are 50 years or older and Florida places within the top 5% of structurally deficient bridges nationally (ASCE Report Card, 2017). Corrosion damage is a primary concern when investigating the service life of aging bridge infrastructure with regards towards the damaging effects chloride induced corrosion has on a bridge bent stiffness, ductility and lateral capacity, especially when placed in bending under lateral loading.

Steel reinforced concrete members in coastal environments undergo damages correlated to chloride ingress, where salt is deposited unto the fascia of piles and piles are cyclically wetted through tidal influence. Moreover, capacity losses accrue from damages attributed to internal chloride ion concentrations within a reinforced concrete substructure, causing reinforcing steel to debond from the concrete, which leads to delamination and/or spalling of cover concrete from the pile or pile cap. Furthermore, substructure components in the tidal zone region, where piles are wetted with salt water, undergoes a continuous evaporative chloride concentration loading process. Salt accumulates on the surfaces of the pile faces and the evaporated seawater deposits an increasing concentration of chloride on the pile faces during low tide. Hence, the tidal region or splash zone in bridge bents often exhibit critical damage because it is highly susceptible to chloride

ingression and consequent corrosion damage. In Florida, the tidal region range is dependent upon a bridge's geographical location, Earth's moon phase, and relevant storm influence. Overall, this process is source of damage because it leads to the reduction of structural integrity, service life, and limit state capacity of bridge substructures.

## **2.2 Corrosion Initiation**

Degradation of reinforcing steel begins once concrete pore water, which is inherently alkaline, is offset by an electrochemical interaction between chloride ions, steel, and concrete. A protective film or passive layer surrounding the reinforcing steel deteriorates when a chloride concentration at the interface of the steel, reaches a critical threshold value ranging from 0.037 - 0.075 lb Cl-/ft<sup>3</sup> (Mindness et al. 2003). Aspects of chloride induced corrosion of steel in concrete includes, the pore water within the concrete that serves as an electrolytic solution and the reinforcing steel itself, that serves as both an anode and a cathode. A half-cell reaction takes place, where oxidation occurs at the cathode and reduction occurs at the anode. Once all requirements for steel to corrode in concrete are satisfied, active corrosion of the reinforcing steel initiates.

Upon meeting the critical threshold required for steel to de-passivate, Iron-oxide reaction products form on the steel surface and volumetrically occupy several times the volume of iron steel unsubverted by corrosion. Pourbaix diagrams for iron illustrate regions where iron in concrete is actively corroding, immune to corrosion or is in a passive state, with respect to pH and voltage potential (ACI 222R-3). The Pourbaix diagram for iron is illustration in Figure 2.1.

A radial tensile stress is exerted on the surrounding concrete as a result of steel actively corroding within a concrete member. This internal stress ultimately spalls the concrete cover, diminishes pretensioning, and circumferentially reduces reinforcing steel area. Concrete that has spalled further exposes otherwise unaffected steel to an extremely aggressive environment.

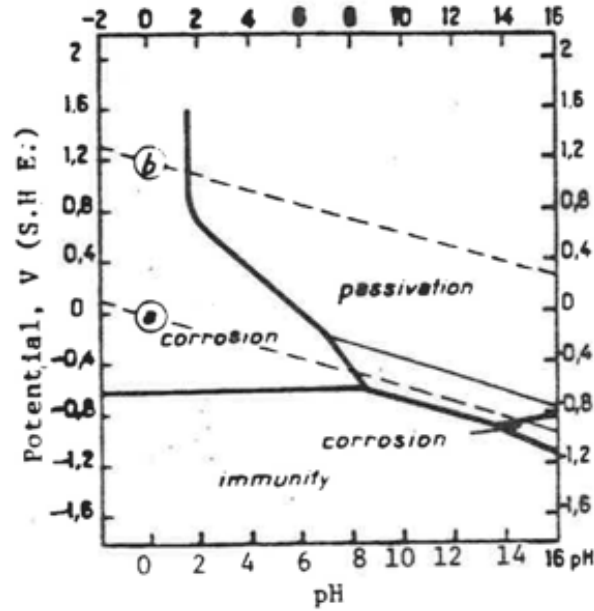


Figure 2.1 Pourbaix diagram for iron (ACI 222R-89).

Shown below is an equation solving for the total time to develop “externally observable damage,  $t_s$ , on a reinforced concrete element. It’s relevance in predicting damage progression with time in reinforced concrete structures subject to steel corrosion damage is important to design and maintenance” (Sagüés 3). Quote, “The time to spall is a function of the ratio of cover to bar diameter, the reinforcement spacing, and the concrete strength” (ACI 222R-3 11).

$$t_s = \frac{x^2}{4D[\text{erf}^{-1}\left(1 - \frac{C_T}{C_s}\right)]^2} + t_p$$

Table 2.1 Calculation parameters.

x	Average rebar cover	76 mm
D	Average apparent chloride diffusion coefficient	$2 \times 10^{-7} \text{ cm}^2/\text{s}$
$C_T$	ECR chloride concentration threshold	$1.55 \text{ kg/m}^3$
$C_s$	Standard deviation of surface chloride concentration	$14 \text{ kg/m}^3$
$t_p$	Corrosion propagation time	yrs

### 2.3 Corrosion Damage of Bridges

Construction practice for coastal bridges built throughout the twentieth century commonly includes a series of collinear square prestress concrete piles, driven into subaqueous soils, until a

developed capacity satisfies required design load criteria. A reinforced concrete cap, cast perpendicular atop a pile group, serves to unify the piles as a collective load-sharing structural bent and transfers superstructure loads into substructure pile components.

Bridges in the northern part of the United States are subject to freeze thaw cycles, where deicing salts are used to rid accumulated snow on the deck surface. Though practical from a vehicular traffic stance, deicing salts essentially create chloride loading on the deck and the concentration of salt at the deck surface eventually influences the reinforcing steel beneath the cover. This ultimately leads to roadway deck cracking and concrete-steel deck delamination.

Bridges in the southern United States are subject to highly aggressive chloride environments, in that they are located within regions of salt or brackish bodies of water and are typically near or at sea level elevation. Consequently, bridge piles, foundations, footings, columns and pier caps deteriorate with respect to the extent of chloride loading. Damage to these structural elements depend on the height at which the element is from the mean high water level and the frequency they undergo a salt deposition process.

## **2.4 Rehabilitation Alternatives**

Commonly suggested repair practices involve the removal and replacement of all chloride contaminated concrete with uncontaminated concrete before the application of a repair material. This is often accompanied by sacrificial anodes used to administer cathodic protection to a corrosion damaged structural system. Even with excellent project execution considered, this method of repair requires extensive procedures that involve high labor costs, which often times control the overall cost of a given bridge restoration project. When compared to an increase in a structural service life, labor cost to remove contaminated concrete and uncertainty in the complete removal of contaminated concrete, this conventional repair alternative is not often fiscally conservative.



Figure 2.2 Pre-repair removal of chloride contaminated concrete.

When compared with common repair construction practice, structural fabrics are relatively easy to install and have been shown to reduce the progression of corrosion damage to a structure. To remedy further progression of corrosion damage to a structural system, external applications of epoxy saturated fabric material have been found to restore losses in structural capacity. Bridge pile bent repairs which utilize low viscosity concrete crack injection epoxy resin, in conjunction with a traditional wet-layup of fibrous wrapped polymer material (FRP) provides additional load resisting stiffness toward a system in response to lateral loading given that the FRP is adequately bonded to the concrete surface of the pile face.

One area of concern in fiber wrapping a bridge bent without fully removing the existing contaminated concrete, is the continual existence of contaminated concrete inherently retained at the surface between the concrete and the reinforcing steel. If the concrete is to remain, the contaminated concrete-steel interface retains its pre-existing electrolytic chloride concentration solution at the reinforcing steel surface.

However, page 16 of ACI 222R states: “waterproof membranes have been used extensively to minimize the ingress of chloride ions into concrete.” Since external sources of chloride ions are waterborne, a barrier to water will also act as a physical barrier to any dissolved chloride ions. In

that, provided an adequate bond of FRP to salt-saturated concrete, the boundary of externally applied carbon or glass fabrics (CFRP or GFRP), respectively, reduces the ingress of additional moisture caused by tidal dependent evaporative cycles inherent of moisture laden environments.

Ease of installation, bond to substrate, material component compatibility, and maintained impermeability, are requirements when considering an ideal waterproofing membrane (ACI 222R p16). Furthermore, “field performance has been found to depend not only on the type of waterproofing material used, but also on the quality of workmanship, weather conditions at time of installation, design details, and the service environment” (ACI 222-3 p14).

Although FRP is not known to stop corrosion altogether, it has been shown to provide a fiscally conservative means to inhibit and reduce the electrochemical processes, detrimental to the service life of marine infrastructure (Winters et al. 2008). Thus, FRP repair may effectively reduce the chloride concentration driving force by decreasing the chloride concentration gradient, administered from build-up of salt deposits on the concrete pile face. Overall, the reduced cost of labor and material in repairing a bent with epoxy-saturated fiber versus a conventional repair and the demand to retrofit existing structures for loading conditions makes the application of FRP to bridge bents a viable, feasible and economical repair alternative.

## **2.5 Pilot Study**

The effect of corrosion damage on lateral pile capacity was investigated in the late 1990s where four 1/3rd scale, five-pile, bridge bents (piers) were tested at various degrees of corrosion distress at the University of South Florida, structural testing laboratory. The amount of steel damage was the same for all piles in a given test and was estimated to be 10, 30 or 50% steel loss. Another test was performed with piles having no steel loss. The bridge bents were subjected to an increasing lateral load while maintaining constant vertical/gravity loads representative of lateral live loading and service axial loading conditions, respectfully.



The reinforced concrete piles had a 6x6in square cross section and were yard casted with 5/16in steel pre-stressing strands. To simulate 50yrs of chloride diffusion into the concrete, typical of many Florida bridges of that age, accelerated exposure conditions were achieved by casting the piles with an accelerative admixture containing a chloride contamination concentration of 3% by weight of cementitious material within a segment, effectively representative of a localized tidal zone. This replicated an evaporative splash zone corresponding to equivalent splash zones, typical of full-scale bridge bent systems subject to marine environments. Impressed current was also used to further expedite the corrosion rate and thus accelerate pile damage.



Figure 2.3 Corrosion cells instrumented on piles.

Figure 2.3 shows cyclically wetted impressed current accelerator equipment attached to the pile face within the designated damage zone region. This condition accelerated measurable reductions in steel area to then be quantified by a percent loss in the area of prestressing steel. Approximate times were calculated to determine the targeted degrees of damage of 0%, 10%, 30% and 50% area loss of steel. Once a 5-pile set achieved the sought level of corrosion damage, it was cast into a reinforced concrete footer and bent pier cap in preparation for instrumentation and testing.

A pile bent's response to lateral loading in bending moment along the length of a pile, is dependent on the geology surrounding the bent, geotechnical properties and extent of structural damage. The inflection point, defined as the location at which any given pile within a bent exhibits zero bending moment, is subject to change position along the length of a pile depending on soil and cap fixity. The location of moment inflection also depends on the bent design, geometric characteristics and extent of corrosion damage, but is often closer to the pile cap point of fixity than the fixity within the soil, which is not as rigid of a connection. For a fixed-fixed end condition in the top and the bottom pile to with a cap and footer, the inflection point occurs at or near the middle of the length of a pile.

The study examined a 5-pile bent configuration where the inflection point location was set at the middle of the pile so that during testing, the portion of the pile above the inflection point would simulate normal pile response, where the damage zone would be located. Figure 2.4 illustrates the inflection points of two bridges in Florida and one predetermined inflection point from the bridge bent model.

The location of the inflection point in Figure 2.4 is with respect to the length from the bottom of the cap to the point of zero bending and to the pile diameter. This gave basis for the methodology in selecting a pile bent configuration such that it accurately represented a scaled version of structural characteristics common to full-scale bridge bents constructed in a similar linear pile configuration. The variable  $d$ , represents the diameter of the pile, which when multiplied by a factor, represents the length of the positive moment region, measured from the bottom of the pile cap to the point of moment inflection.

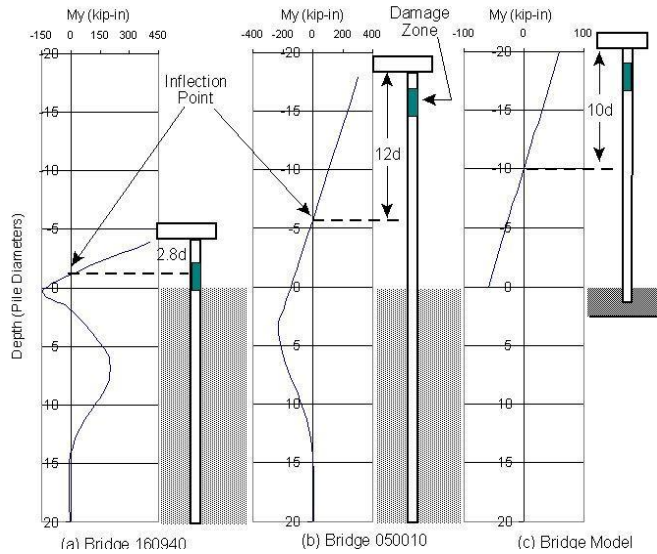


Figure 2.4 Inflection points of Florida bridges and modeled bridge (Goulish, 2002).

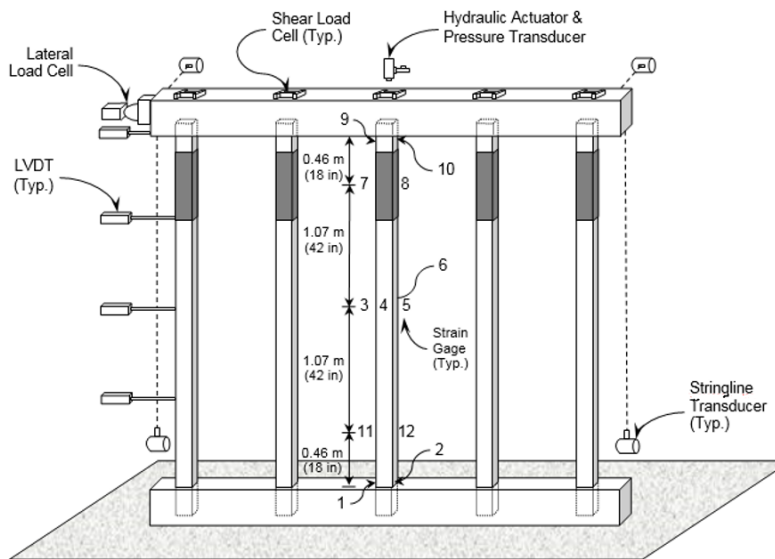


Figure 2.5 Testing instrumentation on pile bent (Goulish, 2002).

Figure 2.5 shows the instrumentation required to measure point specified displacements, test equipment shear resistance, pile stresses and bent lateral translation and bent parallel translation. Hydraulic actuators placed atop the concrete cap directly above the piles, sustained 10 kip axial loads on all five piles. This was regulated though pressure sensor transducers with an automatic pump relay set to maintain 4000 psi in the hydraulic line. Linear variable displacement gauges (LVDT) were placed at quarter points along the pile to measure lateral displacement.

Concrete strain gauges were mounted to determine pile stress in multiple locations along the length of each pile. Shear load cells were used to calibrate lateral displacement of the cap due to friction between the roller cap frame and the concrete specimen.

The prime objective of the study was to assess lateral capacity reduction in pile bents under service dead loads due to lateral loads. The test results indicated that lateral capacity reductions under these conditions were relatively small given the extraordinary level of damage. However, there was considerable reduction in stiffness and ductility in specimens corroded to 30% and 50% that led to sudden and catastrophic failure. Brief details are given below:

- a. 10% Model Bent - the reduction of the ultimate lateral capacity of this bent was barely noticeable at approximately 1% of loss. The load-displacement response however demonstrated a softer response after yielding.
- b. 30% Model Bent - the reduction of the ultimate lateral capacity was more severe at this level of damage, proving to be 13% below the undamaged control. Although the initial stiffness of the load-displacement response was similar to the control, the yield load was reduced by 0.4 kips and its ultimate capacity achieved at a displacement that was 13 mm (0.5 in) smaller. Catastrophic failure in three out of the five piles occurred at a displacement of 89 mm (3.49 in).
- c. 50% Model Bent - the reduction of the ultimate lateral capacity was found to be only 30%. The stiffness of the pile bent was approximately half that of the control and the ultimate capacity reached at a displacement that was 25 mm (1 in) less. Catastrophic failure occurred in all five piles at a lateral displacement of 59 mm (2.31 in), more than 25 mm (1 in) less than in the 30% model bent.

Provided the controlled setting of the experiment, specifically the extent and location of subjected damage to the piles, Table 2.2 provides results from testing and illustrates the increasing trend of capacity reduction with respect to increasing loss of area of prestressing steel. Figure 2.6 illustrates that as a bent is damaged by corrosion, the structure exhibits loss in stiffness, ductility and lateral load carrying capacity. Decreased axial capacity, decreased lateral capacity, and decreased maximum displacements are observable in Table 2.2 and dependent on percentage levels of strand loss in each bent case.

Table 2.2 Max load and displacement response with respect to increasing damage level.

Model Bent	Max. Lateral Load $P_L$		Displacement @ Max. Lateral Load		Maximum Displacement		Capacity Reduction Multiplier
	kips	kN	in.	cm	in.	cm	
Control	9.35	41.6	2.75	7	>5.5	>14.0	1
10% Mass Loss	9.26	41.2	4.17	10.6	>6	>15.2	0.99
30% Mass Loss	7.1	31.6	2.25	5.7	3.49	8.9	0.76
50% Mass Loss	6.58	29.3	1.88	4.8	2.31	5.9	0.7

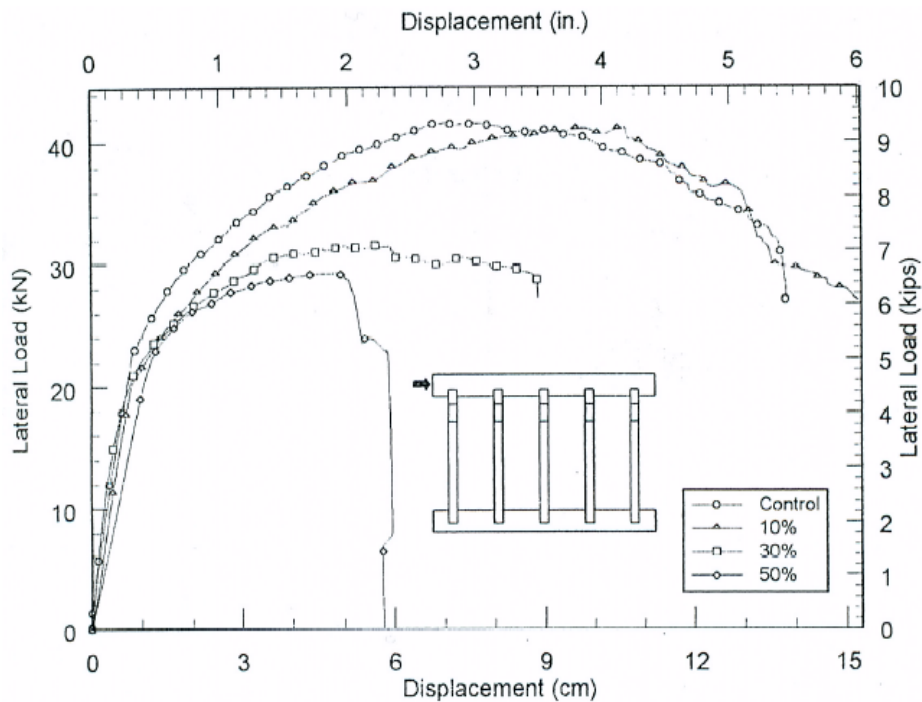


Figure 2.6 Lateral load vs lateral displacement at pile cap (Goulis 2002).

Table 2.3 Undamaged bent measured loss in capacity due to loss in steel area.

Loss in Area of Steel	Percent Reduction of Capacity @Max Lateral Load	Percent Reduction of Displacement @ Max Lateral Load
0%	0%	0%
10%	-1%	52%
30%	-24%	-18%
50%	-30%	-57%

One may conceive from Table 2.3 that as damage within the critical damage zone of pile increases, lateral capacity decreases and the maximum displacement decreases, indicative of a more brittle response to lateral loading as steel area decreases.



Figure 2.7 50% damage bent prior to testing.

Figure 2.7 shows the 50% damaged pile bent configuration inset within the testing frame pre-test and post-test of pile cap severance. Approximately twenty years after the piles were originally cast, a FRP pile repair scheme will be developed with the intent of fully restoring the capacity of the piles and bridge bent to the uncorroded conditions.

## 2.6 Scope of Study

Five corrosion damaged piles, now with far greater than 50% steel loss remain at the outdoor research compound at USF. These provide just enough pile specimens to test a bridge bent, after being repaired with FRP technology. The damage states of the piles vary, but all exhibit extensive cracking in the simulated splash zone. Piles are often times repaired through methods of cracked concrete cover removal, then formed back to the original dimensions. This approach however, cannot reintroduce existing structural load into the repair without jacking up the bridge during repair, then releasing the load into the newly repaired piles.

To minimize disturbance to the cover material for at least four of the five piles, the following steps are envisioned: cleaning, patching cracks at the surface, injecting internal cracks with a highly mobile epoxy, and providing a structural CFRP wrap to restore the bending capacity, assuming 100% steel loss might exist.

The objective of this study is to model and design the repair required to restore ultimate axial and bending capacity to a heavily corroded one-third scale prestressed 5-pile bent. This would then lay the groundwork for the future FRP repair and laboratory testing of the 1/3rd scale bridge bent.

Figure 2.8 is a plan view of the existing piles that indicates their position at the USF civil engineering research facility and their identification markings. Figure 2.9 is an elevation view of the test bent. Figure 2.10 provides the reinforcing scheme of the pile cap for the test bent. Both Figure 2.9 and 2.10 replicate the dimensioning used in the past experiment in order to isolate variability in testing results.

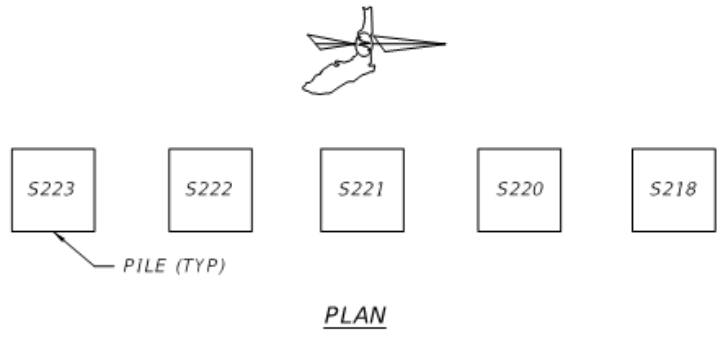


Figure 2.8 Existing pile identification.

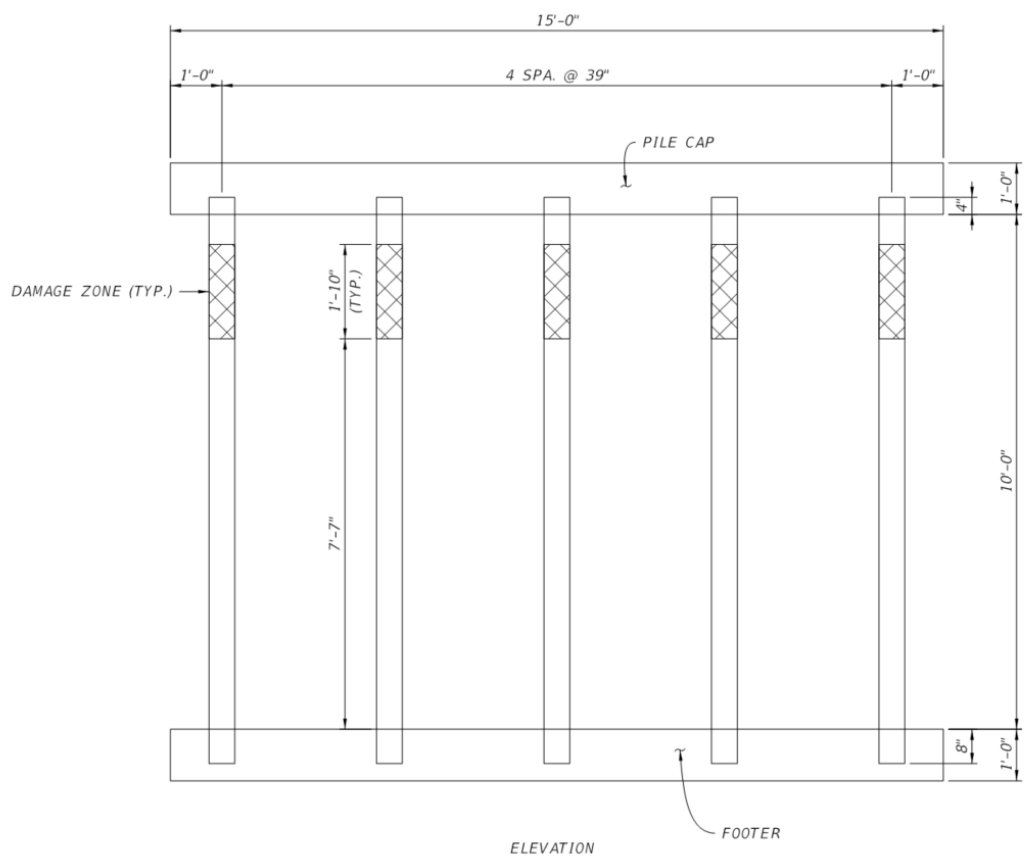


Figure 2.9 Elevation view of bent.

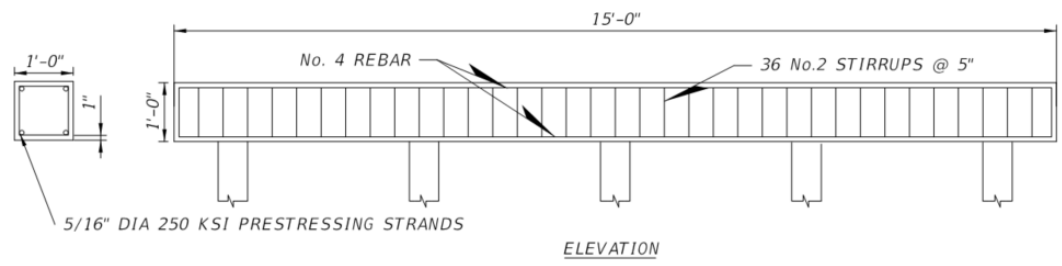


Figure 2.10 Pile and cap reinforcing scheme.



## **CHAPTER 3: MODELING CORROSION DAMAGED PILE BENTS**

This chapter details the use of FLPIER software to model corrosion damage and the repair of corrosion damage to bridge pile bents with respect to lateral capacity subsequent to loss in effective area in prestressing steel. The variables considered to construct the model skeleton were analyzed with respect to the degree in which they affected the models structural response. This is in reference to the measured control structural response test data via lateral load-displacement curves. Once a model satisfied a response within a tolerance from that of the measured control bent testing response from the pilot experiment, it was designated as the control model. Models that represent damage are subsidiary to the control model in that they possess identical control variables and vary only in the severity of corrosion damage at which they are run.

### **3.1 FLPIER**

FLPIER is a non-linear analysis software program that prompts users to input geological soil profiles, geotechnical material properties, structural load combinations and structural material properties. In specific, the program non-linearly, segmentally analyzes a structural response to user defined load cases and input parameters. The purpose and application, within this study, is to accurately model the measured experimental data (signal match) in order to institute an adequate repair design, material selection, and testing procedure.

To be discussed are parametric evaluations and descriptions of model-runs, where the basis of accuracy in observing model behavior directly references the measured lateral-load structural response from the previous study. Therein, signal matching is the process whereby the measured

load vs displacement is used as a comparison and where a model is adjusted until modeled response matches that with was measured.

### **3.2 Model Assumptions**

To maintain tolerable and sound scientific reasoning for both damaged and repaired models, while adhering to software limitations, it is assumed that a variety of structural response influencing variables are simplified to geometrically designated segment lengths. After having modeled the pile group to its exacting nature, the overlay of accounted variables and the nodes at which FLPIER analyzes a structure, ultimately lead the model to indefinitely iterate. This gave basis for simplification of both the control model and subsequently the damaged and repaired models.

FLPIER is programmed to analyze a pile along its length with 17 nodes or 16 segments per pile Figure 3.1 illustrates the nodal configuration for all designed models. The length of a pile in FLPIER begins at the bottom of the substructure pile cap and ends at the toe of the pile. This discretization also assigns one segment between the bottom of the pile cap and the beginning of soil. The remaining 15 elements are equally spaced longitudinally within the highly indeterminate soil layers.

For this project, eight segments with varied cross sectional parameters were overlain within the 16 available sections. This provided a means to input changes in cross section strengths, resulting from loss of steel, steel prestress and concrete precompression.

Influencing variables, including geometric characteristics, pre-stress transfer length, moduli of elasticity, and steel stress levels, were simplified to reside within the confines of the fixed-nodal characteristics governing FLPIER.

### 3.3 Influencing Variables and Input Parameters

All considered variables were analyzed and assigned a variable influence weight through a series of model run-trials. Curve fitting by trial allowed for determination of how to conservatively simplify a pile group model with respect to a repair model and repair design.

Table 3.1 Model input parameters.

Prestressing Steel		
$E_s$	29000	ksi
Area/ Strand	0.059654808	in <sup>2</sup>
Number of Strand	4	
Prestress	150	ksi
Steel Adjustments		
AOS	0.05965	in <sup>2</sup>
Target Force/Area	192.78	ksi
Yield Strength	250	ksi
Ratio	0.771	
Prestress	150	ksi
Adjusted prestress	192.78	ksi
Concrete		
b	6	in
h	6	in
Gross Area	36	in <sup>2</sup>
Area	35.8	in <sup>2</sup>
Stress in Concrete	1	ksi
Uncontaminated Concrete		
$f_c$	8.5	ksi
$E_c$	5255140	psi
$E_c$ (Inflation%)	5255	ksi
Contaminated Concrete		
$f_c$	5.5	ksi
$E_c$	4227233	psi
$E_c$ (Inflation%)	4227	ksi
Cap Concrete		
$f_c$	6	ksi
$E_c$	4415201.0	psi
$E_c$ (Inflation%)	4415.2	ksi

Table 3.1 represents parameters used in developing determining an adequate curve match and provided the basis for values used within the FLPIER models to achieve a conservative CFRP repair design. Figure 3.1 illustrates the nodes at which FLPIER performs analysis within the constructed structural system.

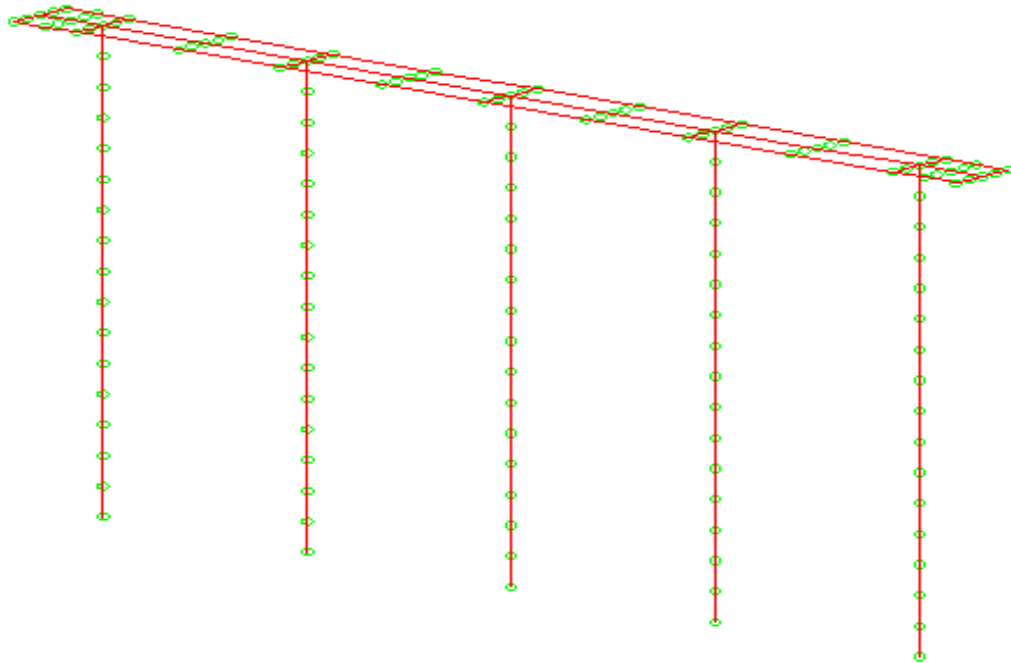


Figure 3.1 FLPIER nodes.

### 3.4 Modulus of Elasticity of Concrete

The modulus of elasticity values used within the models had the most significant effect on the model stiffness concerning the bents elastic response during lateral loading. Beyond the elastic limit of the system, the models indicated a decreasing trend to a damaged bents ductility when compared to increasing damage levels.

Section 19.2.2 of ACI 318-14 states that “The modulus of elasticity for concrete is sensitive to the modulus of elasticity of aggregate and mixture proportions of the concrete. Measured elastic modulus values can range from 80 to 120 percent of calculated values” (ACI 318-14 315).

From the above statement, the initial damage model's cap and piles were swept with the suggested measured elastic modulus percent range. The inflation and deflection percentage applied to the average measure concrete compressive strength provided a range of curves that was used to isolate an influencing variable that may result in deviations from accurate displacement model data analysis. Figure 3.2 illustrates that within the elastic region of the curve, a model run with a concrete compressive strength at the high range of 20% inflation, results in a curve that is elastically similar to the measured undamaged control model. In subsequent repair models, no moduli inflation percentages were considered as to apply a conservative assumed stiffness to the repaired models.

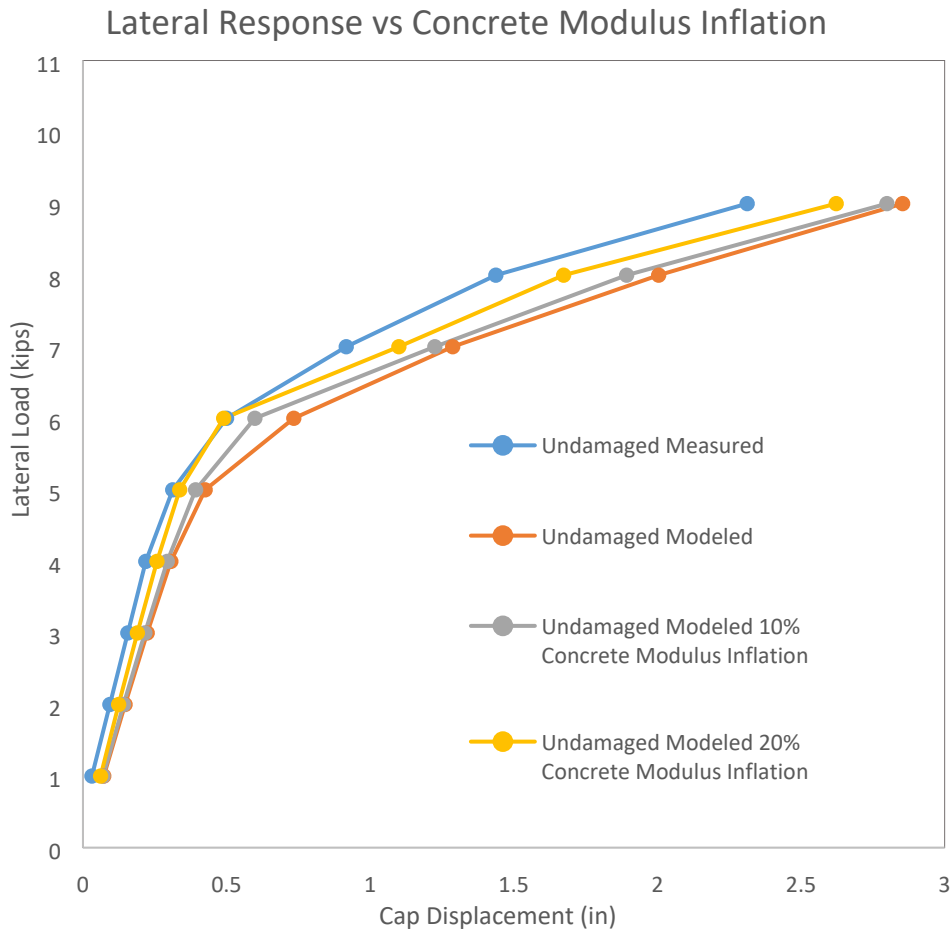


Figure 3.2 Modeling undamaged bent varying concrete modulus.

Prestress input values in units of ksi within a designated segment were solved through the force equilibrium between prestressing strand tension and concrete compression target and actual stress. The target prestressing force in the pilot study and in modeling the study was 11.5 kips, where within the model, a value of 1ksi is assumed for the target concrete precompression stress.

The mathematical model to follow (Figure 3.3), assumes adequate bond between the prestressing strands and the core of the concrete. It represents prestress loss force equilibrium accounting for loss in effective area of prestressing strands due to corrosion. Table 3.3 assumes a 70% prestress pull factor to 250 ksi prestressing strands and assumes no inflation percentage to the concrete modulus in preparation for the input of conservative parameters leading toward the repair design.

$$F_s = F_c$$

$$\Delta\sigma_{st} = \Delta\sigma_c \frac{E_s}{E_c}$$

$$A_s(150 + \Delta\sigma_{st}) = (1 + \Delta\sigma_c)A_c$$

$$150 + \Delta\sigma_{st} = (1 + \Delta\sigma_c) \frac{A_c}{A_s}$$

$$\Delta\sigma_{st} = \frac{A_c}{A_s} + \frac{A_c}{A_s} \Delta\sigma_c - 150$$

$$\Delta\sigma_c \frac{E_s}{E_c} - \Delta\sigma_c \frac{A_c}{A_s} = \frac{A_c}{A_s} - 150$$

$$\Delta\sigma_c = \frac{\frac{A_c}{A_s} - 150}{\left(\frac{E_s}{E_c} - \frac{A_c}{A_s}\right)}$$

Figure 3.3 Stress/Force change with respect to area of prestressing steel.

Table 3.2 Percent area loss with respect to effective area of steel.

Loss (%)	Area Steel/Strand (in <sup>2</sup> )	Area steel (in <sup>2</sup> )	Ac/As	Es/Ec
0	0.05965	0.23862	149.87	6.931
10	0.05369	0.21476	166.52	6.931
30	0.04176	0.16703	214.10	6.931
50	0.02983	0.11931	299.74	6.931
90	0.00597	0.02386	1498.68	6.931

Table 3.3 Percent area loss with respect to loss in steel prestress.

Loss (%)	Delta Concrete Stress Δc (ksi)	Delta Steel Stress Δ st (ksi)	Concrete Stress (ksi)	Steel Stress (ksi)	Concrete Force (kips)	Steel Force (kips)
0	0.0009	0.006	1.00	150.01	35.79	35.79
10	-0.1035	-0.717	0.90	149.28	32.06	32.06
30	-0.3094	-2.145	0.69	147.86	24.70	24.70
50	-0.5114	-3.545	0.49	146.46	17.47	17.47
90	-0.9041	-6.266	0.10	143.73	3.43	3.43

### 3.5 Prestress Transfer Length

In pretensioned elements, the prestressed force transfers to the concrete by bond over a specific length. This length is referred to as the transfer length. Section 7.6.4.2C states, “The effect of a severed tendon will be effective after a development length is achieved and the full strength of the tendon will be reestablished” (ACI 562-13 37). ACI 318-14 defines that in pretensioned members,  $l_{tr}$  the transfer length of prestressed reinforcement is calculated through Eq. (21.2.3) within the chapter as follows:

$$l_{tr} = \left(\frac{f_{se}}{3000}\right)d_b$$

where,

$f_{se}$  = the effective stress in the prestressed reinforcement after allowance for all losses in psi.

$d_b$  = the nominal diameter of bar, wire, or prestressing strand in inches.

Applying this equation to this experimental condition results in the following prestress transfer length, where  $d_b$  is dependent on the extent of damage to a strand and where  $f_{se}=150$ ksi.

Applying this equation to the parameters of this experiment is shown below for two conditions.

For undamaged prestressing steel condition:

$$l_{tr} = \left(\frac{150,000}{3000}\right)(0.2756) = 13.78 \text{ inches}$$

For 90% prestressing steel area loss condition:

$$l_{tr} = \left(\frac{150,000}{3000}\right)(0.2614) = 13.07 \text{ inches}$$

Experimental research practice indicates a prestressing strand's transfer length is approximately equal to 60 to 100 times the diameter of a strand, after allowance for all losses. However, as a strand becomes damaged by corrosion, its volumetric cross-sectional area increases, while its effective cross-sectional area decreases. This aspect of damage allots for a degree of uncertainty in determining the length in which a given prestressing strand is able to adequately transfer a target concrete precompression stress value of nearly 1 ksi. Table 3.4 illustrates prestress transfer lengths provided a variable transfer length range for a stand undamaged by corrosion.

Table 3.4 Diameter of stand multiplication factors.

Diameter X	Diameter Strand (in)	Transfer Length (in)
60	0.3125	18.75
70	0.3125	21.87
80	0.3125	25.00
90	0.3125	28.12
100	0.3125	31.25

The control model was swept with varying prestress transfer lengths and cross-referenced with measured lateral load vs lateral cap displacement curves. It is assumed for all models to have a transfer length of 16 inches measured from the bottom of the cap, which does not correspond to 70 x diameter of a strand exactly, but is reasonable to assume provided the level of uncertainty in the extent of steels damage influence on transfer length. This approximation is within reason to the calculated transfer length from ACI 318-14, and geometrically fits within the allotted 8in per



segment located 16 inches from the bottom of the cap to node 3. This length also takes into account the 4 inches of pile embedment into the cap when referencing into FLPIER.

Conclusively, it was decided to set the overall prestress transfer length to equal the length of two segments within the model, which corresponds to two 8 inch segments, totaling a 20 inches, with a 4-inch pile cap embedment and a target prestress value of 150ksi. Therefore, cap embedment included, the actual transfer length input used for all models equals 20in, which corresponds to nearly 70 times the diameter of the strand.

### **3.6 Undamaged Control Model**

The control model first consisted of 11 segments where all of the models variables were input geometrically precise. Once the model was retrofit for the repair, the models would not account for the exacting precision. Thus a decision to approximate the segments such that the variables fit within reasonable tolerance of acceptable segment lengths. This resulted in a model consisting of 8 segments, where there is one large segment after the prestress was considered fully transferred. The damage region prestress values were edited with respect toward loss of effective prestress due to loss of reinforcing steel area. Seven segments are 8 inches in length and one segment is 72 inches in length.

This geometrical simplification allowed for accurate representation for all variables and gave rise to the repair model baseline. Figure 3.5 illustrates the final pile segment configuration used throughout all of the models. It is the result of simplification to segmentation of the model in order to reflect all of the investigated influencing structural parameters with respect to the damaged region and pile bent response when place under lateral load.

FLPIER analyzes a pile group only if the group is embedded in soil. Since the experimental bent is not tested in soil, and instead has a footer, the soil used to replicate the experiment test within the model reflects soil properties of which a pile group is essentially embedded into the

actual base of the frame. Low strength sand soil was used with minute strength characteristics in the region where the piles are to exhibit no resisting soil conditions. Stiff clay with inflated properties near that of concrete was used for the embedment of the concrete footer. Figure 3.4 and Figure 3.5 show the elevation view of the bent embedded in soil with respect to respective geotechnical soil properties used within all models.

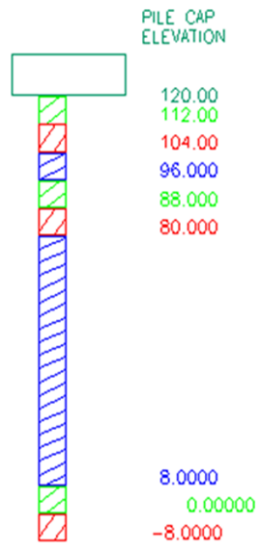


Figure 3.4 Control model segments elevation view (ft).

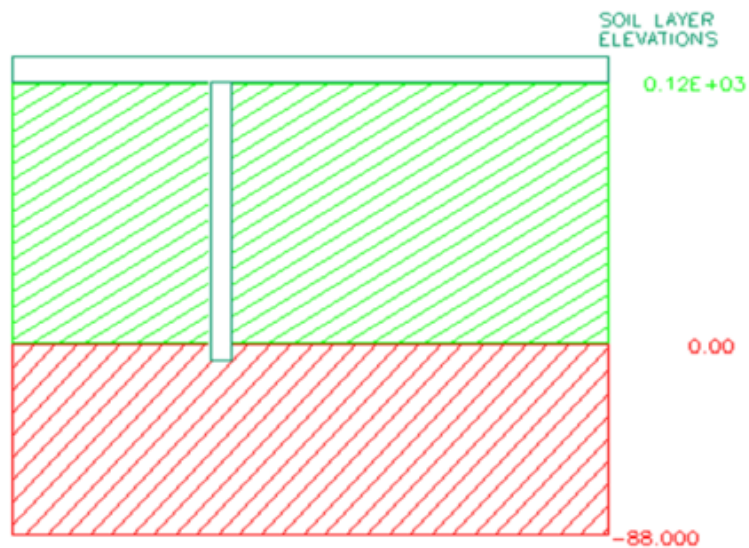


Figure 3.5 Geotechnical characteristics of FLPIER model (ft).

The undamaged model, used as a basis for damaged models and subsequently repaired bent models, utilized the parameters outlined throughout the preceding chapter three sections. As noted, the undamaged model was generated to replicate laboratory testing results referenced to the previous study. Figure 3.6 illustrates the measured structural response versus the models structural response for the undamaged pile bents.

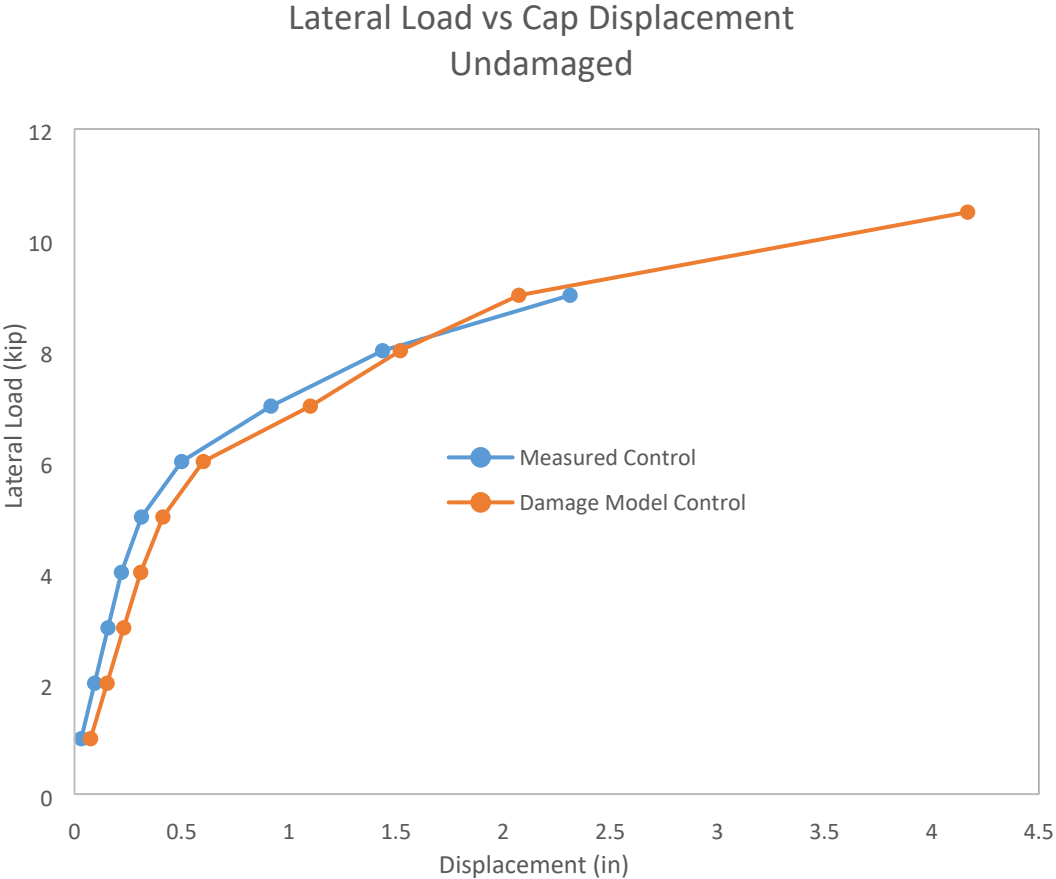


Figure 3.6 Measured vs undamaged model load-displacement curve.

The figures to follow illustrate post analysis results from the undamaged model. The maximum lateral load equals 10.5 kips and the maximum shear within the bent occurred in pile 1 at nearly 2.2 kips. The maximum moment of 12 k-ft occurred at the foot of pile 5. The maximum deflection occurred in Pile-1 at 2.1 kips.

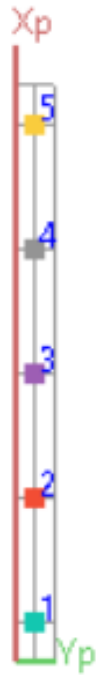


Figure 3.7 Pile count and coordinate orientation.

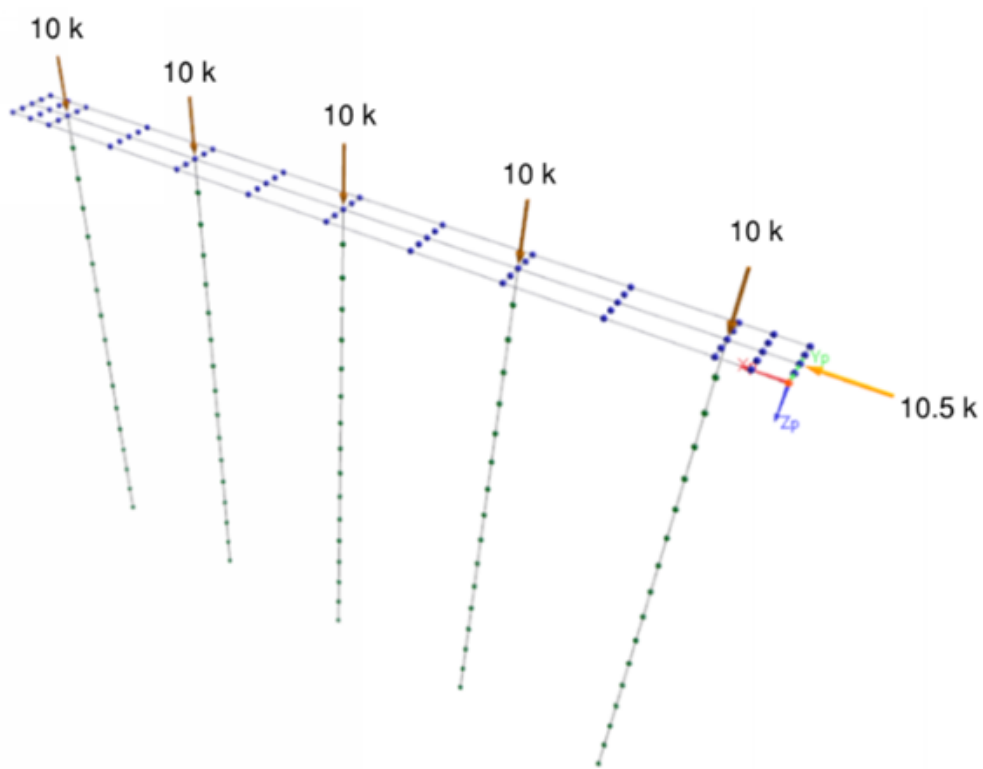


Figure 3.8 Undamaged model with sustained service loads and at ultimate lateral load.

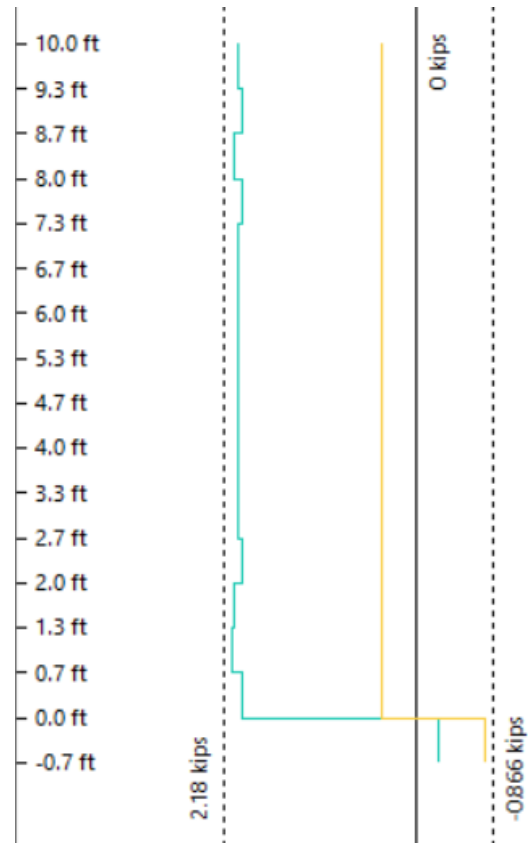


Figure 3.9 Undamaged model max shear.

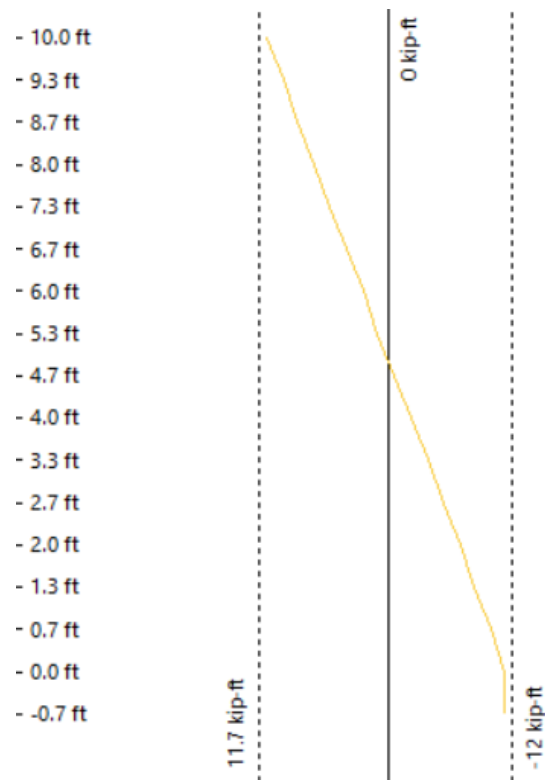


Figure 3.10 Undamaged model max moment.

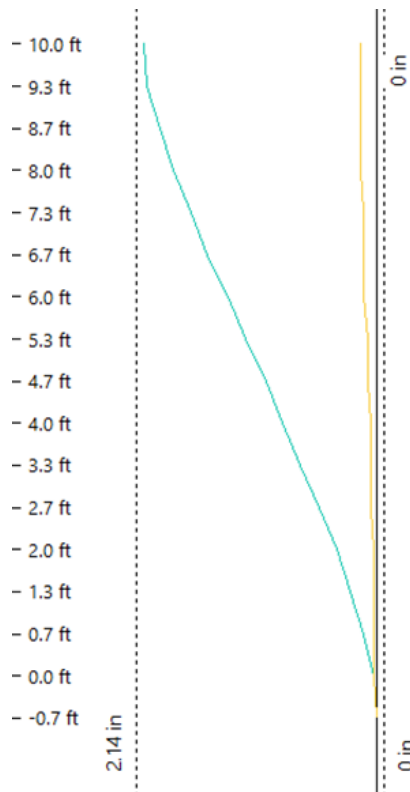


Figure 3.11 Undamaged model max displacement.

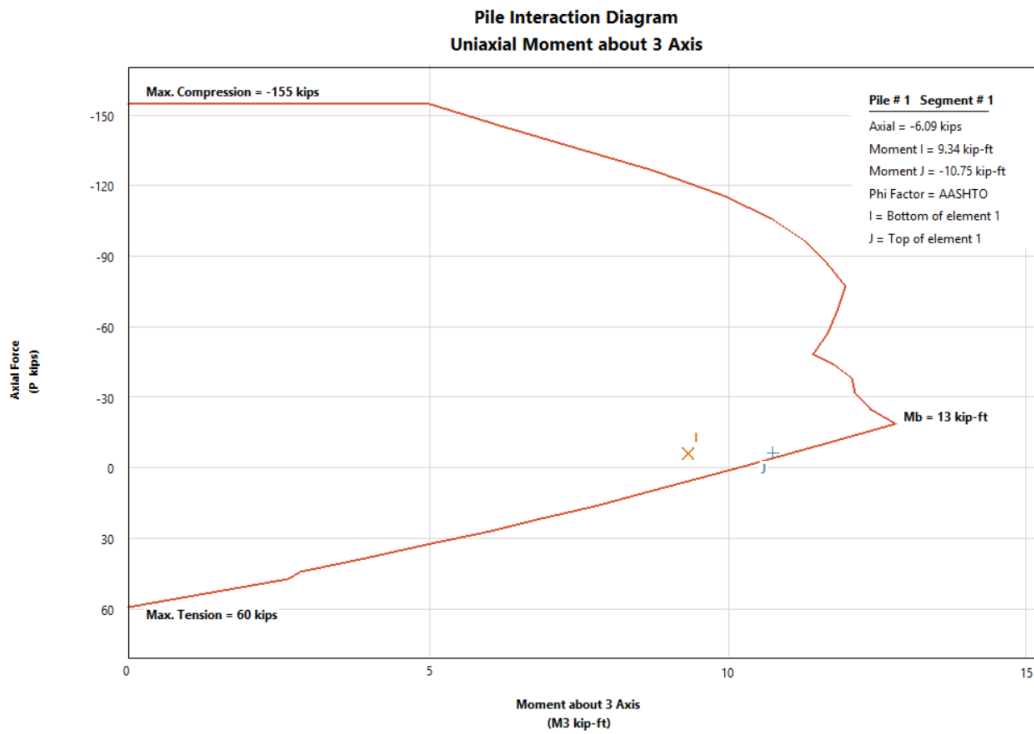


Figure 3.12 Interaction diagram for load case 10.

### 3.7 Damaged Models

Once the determined control model was set as a basis, models were run with increasing damage and lateral load vs displacement curves and interaction diagrams were generated and compared with the control model. Figure 3.13 and Figure 3.14 illustrate the response to lateral loading and the developed capacity with respect to increasing levels of damage, respectively.

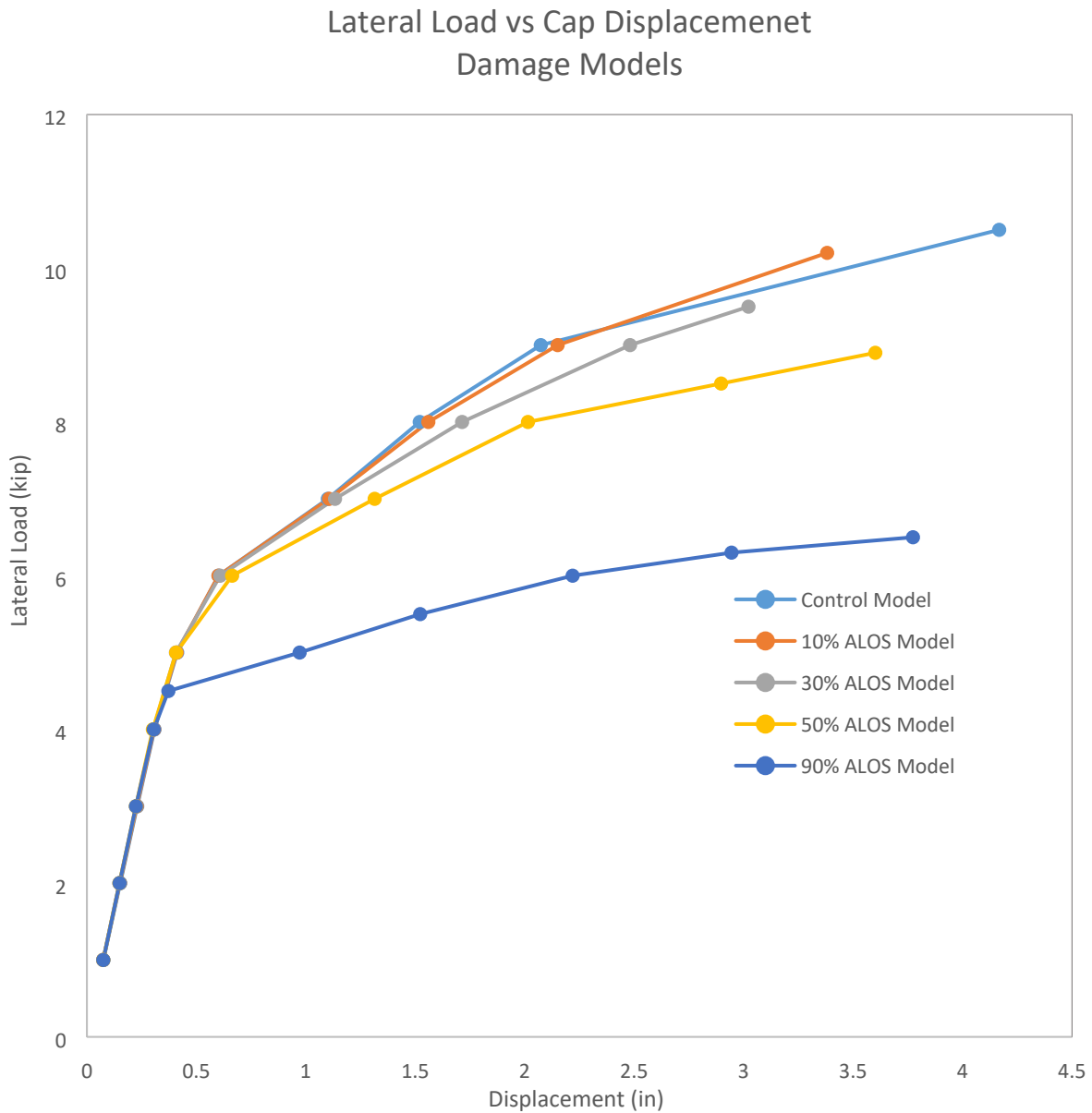


Figure 3.13 Response curves for all models.

### Pn vs Mn Damage Models

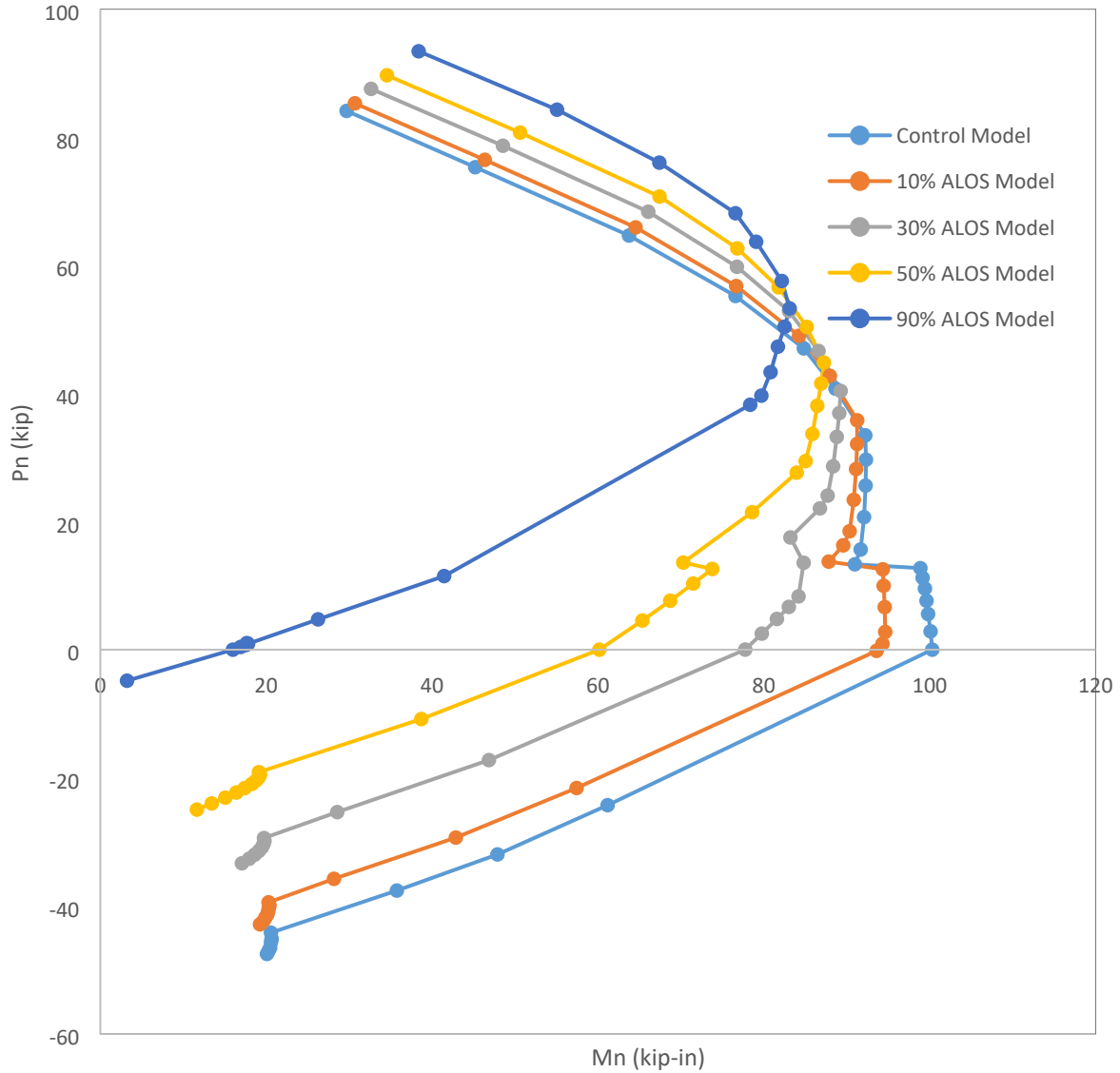


Figure 3.14 Interaction envelope for all models.

The following plots and figures illustrate maximum loading scenarios for various structural responses. The figures to follow demonstrate pile position within the bent, sustained axial loads and maximum lateral load, axial pile response, lateral displacement response, and shear and bending responses with respect to damage at 90% area loss of steel within the damage region.



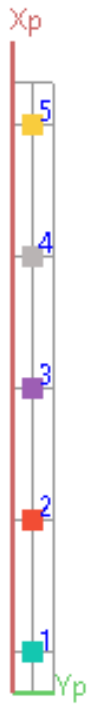


Figure 3.15 90% damaged pile count.

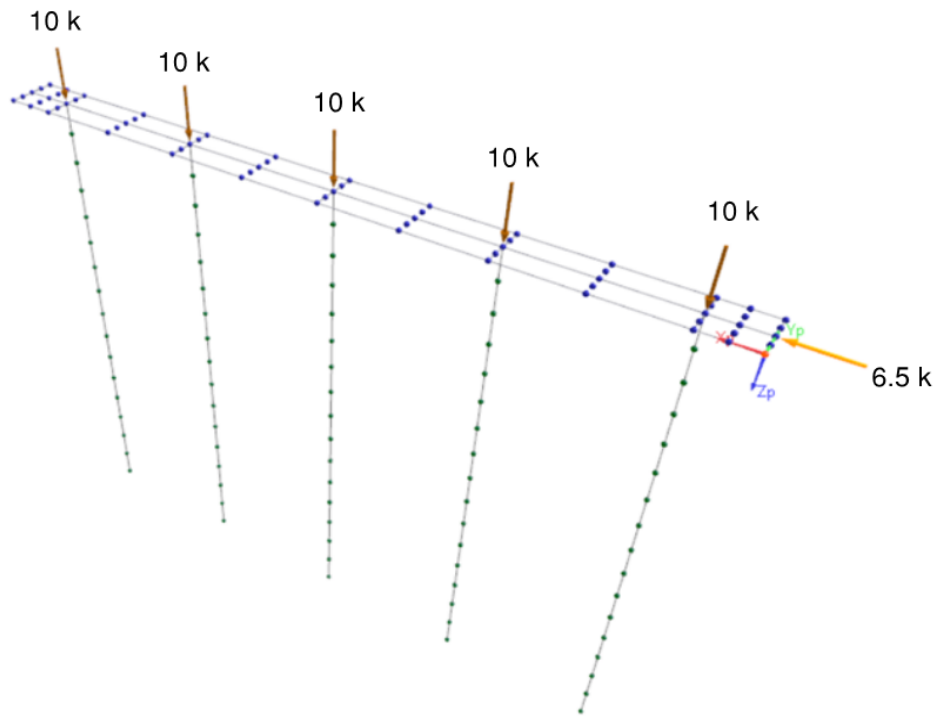


Figure 3.16 90% damaged model sustained service loads and ultimate lateral load.

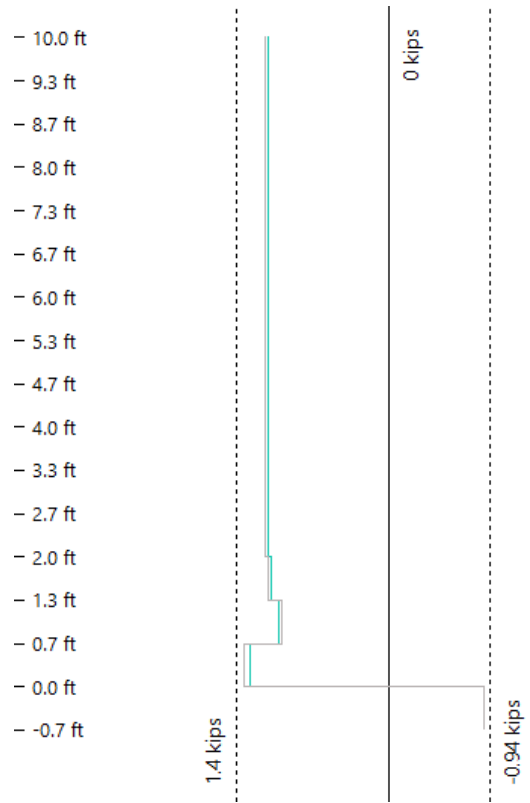


Figure 3.17 90% damaged model max shear.

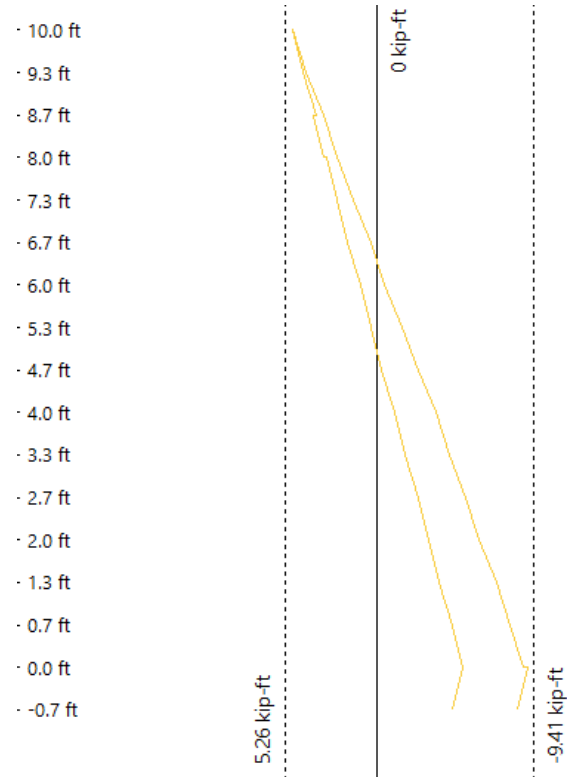


Figure 3.18 90% damaged model max moment.

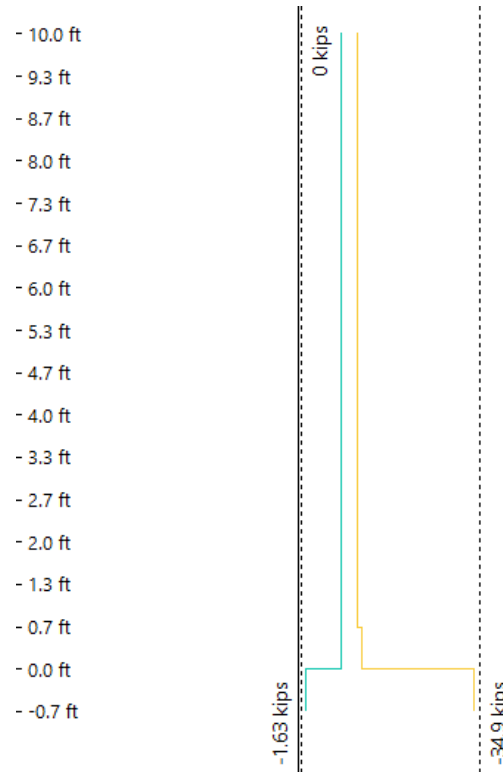


Figure 3.19 90% damaged model max axial force.

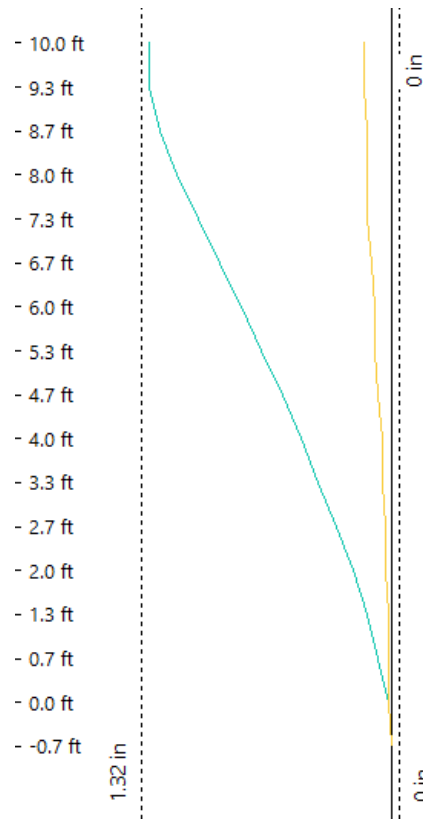


Figure 3.20 90% damaged model max displacement.

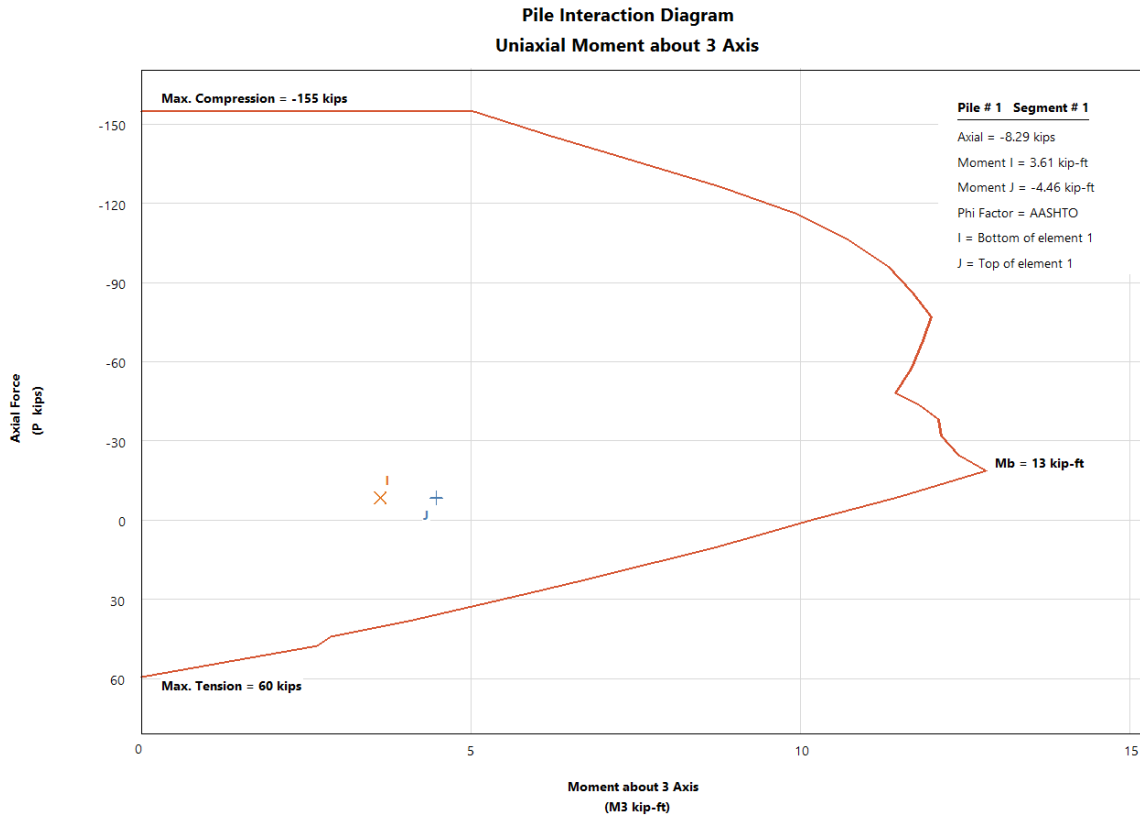


Figure 3.21 Interaction diagram 90% damaged model at load case 10.

Damaged models representative of 10%, 30%, 50% and 90% area loss are illustrated in Appendix B. The damage model with 90% area loss of steel is shown because the current condition of the piles represents greater than 50% loss. To remain conservative in designing for a CFRP repair, it was assumed that the prestressing steel has only 10% effective area of prestressing steel. The 90% area loss of steel damage model was then used to create a repair model utilizing layers of CFRP wrap.

Although bridge bents known to have damage of nearly 20% area loss of steel or greater are generally queued for replacement, often time's knowledge of a bridges damage state is limited until a bridge inspection is performed. Thus, FRP repair is particularly useful in emergency bridge repair scenarios. Table 3.5 provides a summary of results from the control undamaged model and a compilation of models run with identical skeletons.

Table 3.5 Results of damages to models pile bents at max lateral load.

Damaged					
Damage (%)	0%	10%	30%	50%	90%
Shear (kip)	2.18	2.1	2.01	1.83	1.4
Displacement (in)	2.14	2.06	1.85	1.74	1.32
Axial (kip)	51.1	-44.4	-45.8	-39.6	-34.9
Moment (k-ft)	-12	-10.9	-11.2	-10.8	-9.41
Max Lateral Load (kip)	10.5	10.2	9.5	8.9	6.5

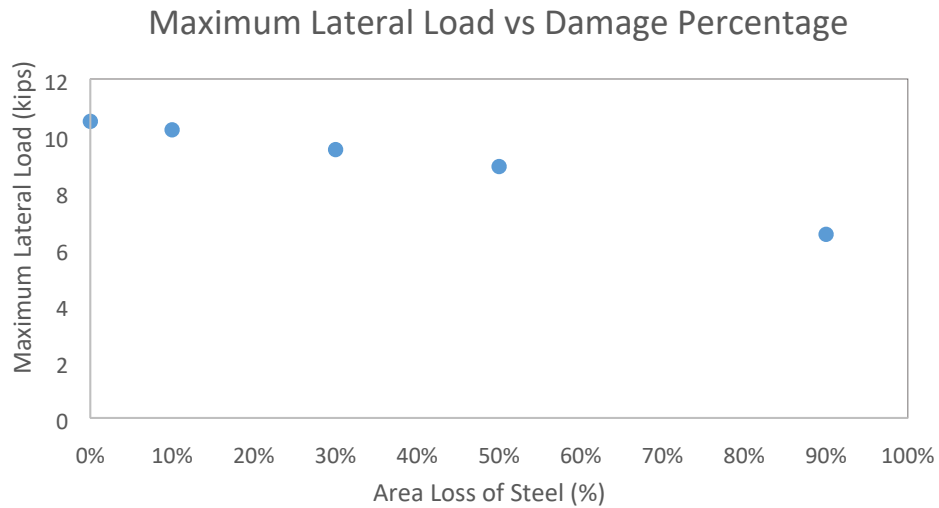


Figure 3.22 Maximum applied lateral load with respect to loss in steel area.

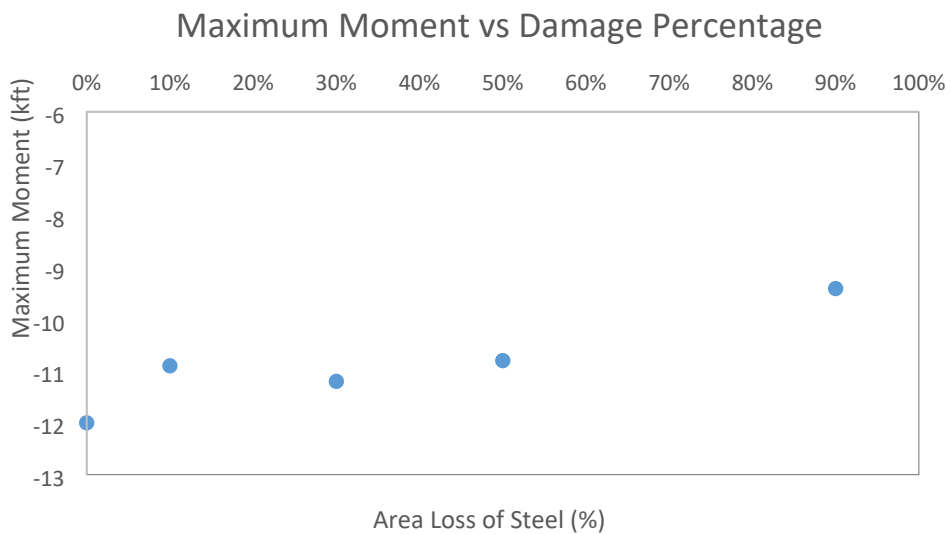


Figure 3.23 Maximum moment in bent with respect to loss in steel area.

Maximum Shear vs Damage Percentage

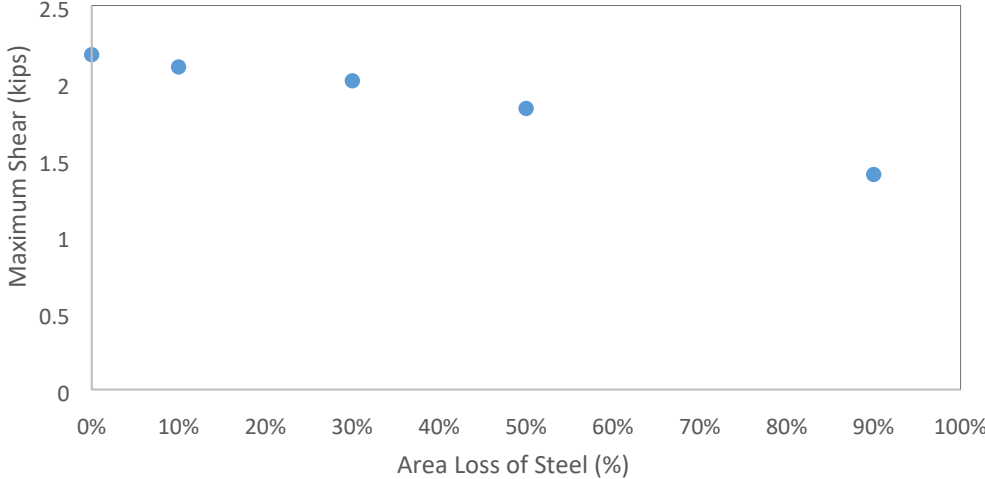


Figure 3.24 Maximum shear in bent with respect to loss in steel area.

Maximum Lateral Displacement vs Damage Percentage

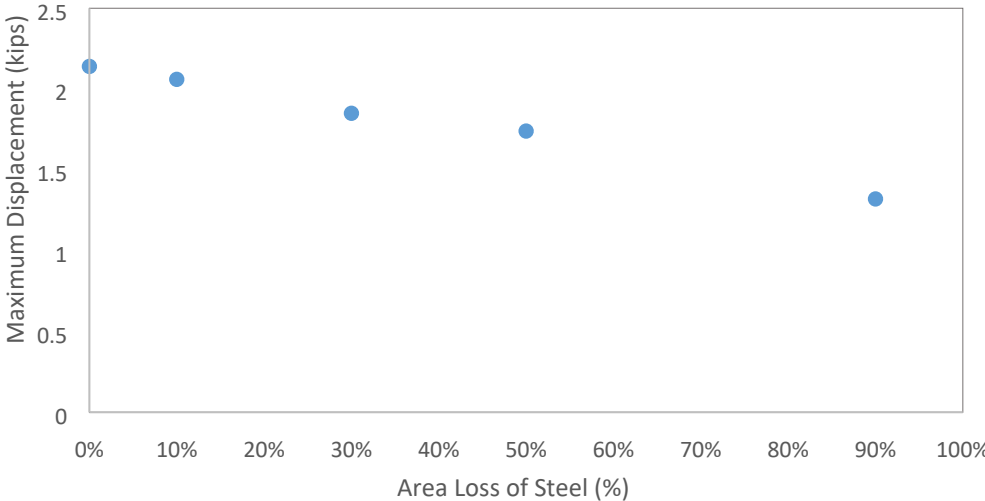


Figure 3.25 Maximum lateral displacement in bent with respect to loss in steel area.

## CHAPTER 4: MODELING FRP-REPAIRED PILE BENTS

Interaction diagrams were developed and used to interpret the efficacy of the number of CFRP plies for a satisfactory repair. Lateral load versus lateral displacement of the cap was analyzed using FLPier to model the reinstatement of lateral capacity through use of CFRP near the exterior of the cross section of the five piles.

Figure 4.1 illustrates the three layers of repair which effectively is modeled as two layers because the third layer does not assume to provide bending resistance to the structural system but instead provides passive confinement and shear resistance.

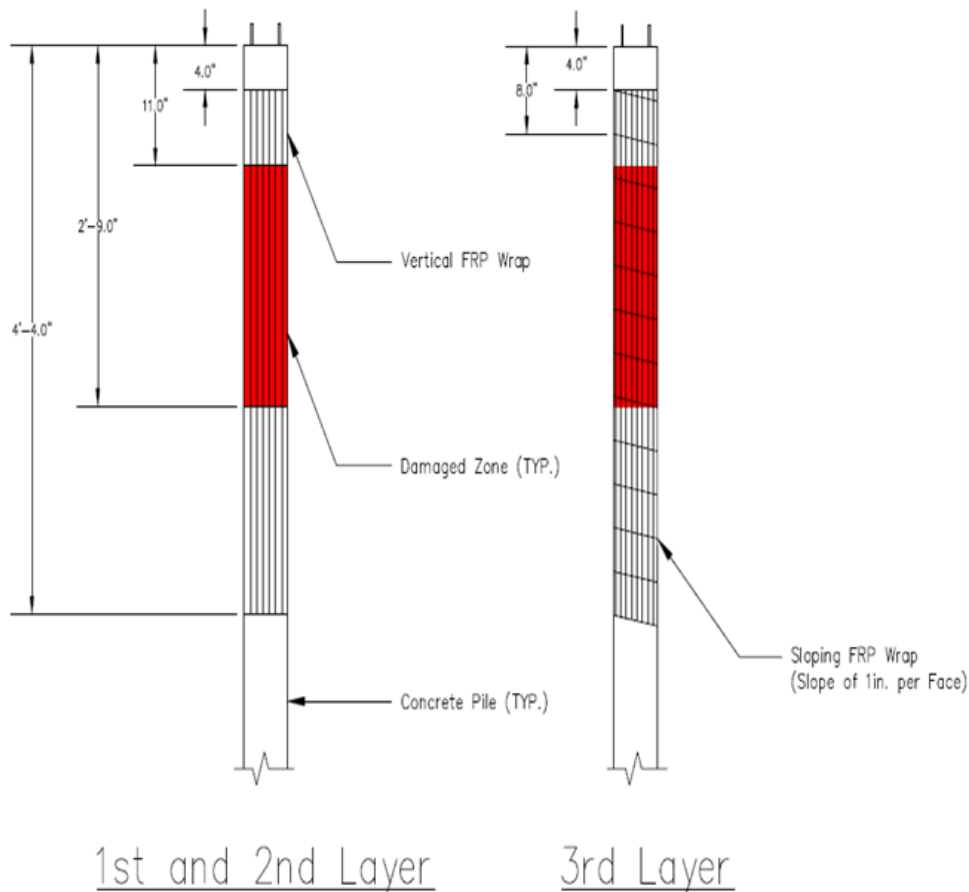


Figure 4.1 CFRP design schematic.

#### 4.1 CFRP Tensile Design Calculation

A calculation for an approximation to determine the number of plies was performed in conjunction with software analysis. The following calculation is for tensile capacity design considerations assuming 100% loss in steel area.

Strength of one prestressing strand=14.9 kips
Depth of Existing Reinforcement $\approx 5$ in
Distance from one compression block to fiber = $d - \frac{a}{2} = 4.5$ in
Moment capacity=14.9 kips*(2 Strands)*4.5 in = 134 k-in
Distance from compression block to fiber = 5.5 in
Required Carbon Force Total = $\frac{134 \text{ k-in}}{5.5 \text{ in}} = 24.4$ kips
Required carbon force per inch width = 4.06 kips

Figure 4.2 Strength requirements for repair material.

Since the carbon fiber selected produces a tensile average ultimate strength value of 7.2kips/in width, then only one layer is required to satisfy the loading conditions. However, two longitudinal layers were selected in order to reside within a conservative design.

#### 4.2 Repair Models and Carbon Shell Distribution

CFRP properties were simulated within the repair models by defining arbitrary “mild steel” with material properties of carbon fiber. A shell was created around the outside of the pile cross-section through a calculation that provided a bar diameter equivalency. Fifty to 60 bars were tightly spaced with properties corresponding to carbon fiber. The thickness of the material was used from the specification sheet to define the area to be used to create the FRP shell.



Repair models used what is called “mild steel” within the program. These groups of steel are listed within the .in file as groups 3-6. Each group is located on the exterior of each of the pile cross-section, 2.9in from the center of the square cross-section. The repair groups are representative of the materialistic properties of the repair materials selected. Each repair group has 50 circular carbon bars distributed along the 6-inch dimension of each face of the piles amounting to 4 faces per pile and five piles in total. Figure 4.3 shows a repaired models cross section, where an added exterior layer was applied by inputting structural properties of carbon fiber material and distributing the repair material area over the width of the cross section.

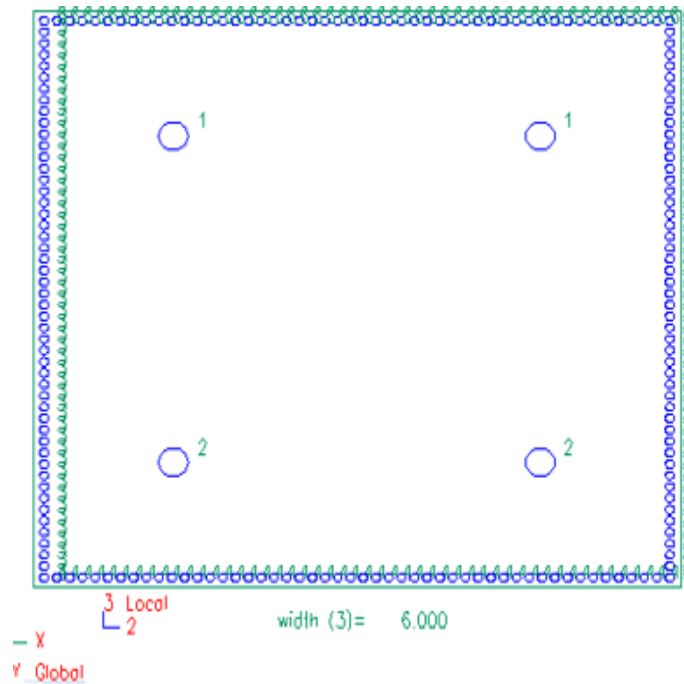


Figure 4.3 Square cross section with custom reinforcement.

Repair models included all stages of damage: 0%, 30%, 50%, and 90%. The models implement a single ply unidirectional carbon fiber fabric laid parallel to the pile. The following figures illustrate maximum values during load case 10 for the 90% damaged bent. Load case 10 represents the largest lateral load that is able to be placed on the bent structure.

Table 4.1 Model results for single ply CFRP repair with respect to damage.

Single Ply Repair				
Damage (%)	10%	30%	50%	90%
Shear (kip)	2.38	2.29	2.51	2.49
Displacement (in)	2.06	1.98	2.8	3.09
Axial (kip)	-40.8	-39.6	-39.5	-49.1
Moment (k-ft)	-14.2	13.5	14.2	14.3
Max Lateral Load (kip)	11.6	11.1	12.5	11.9

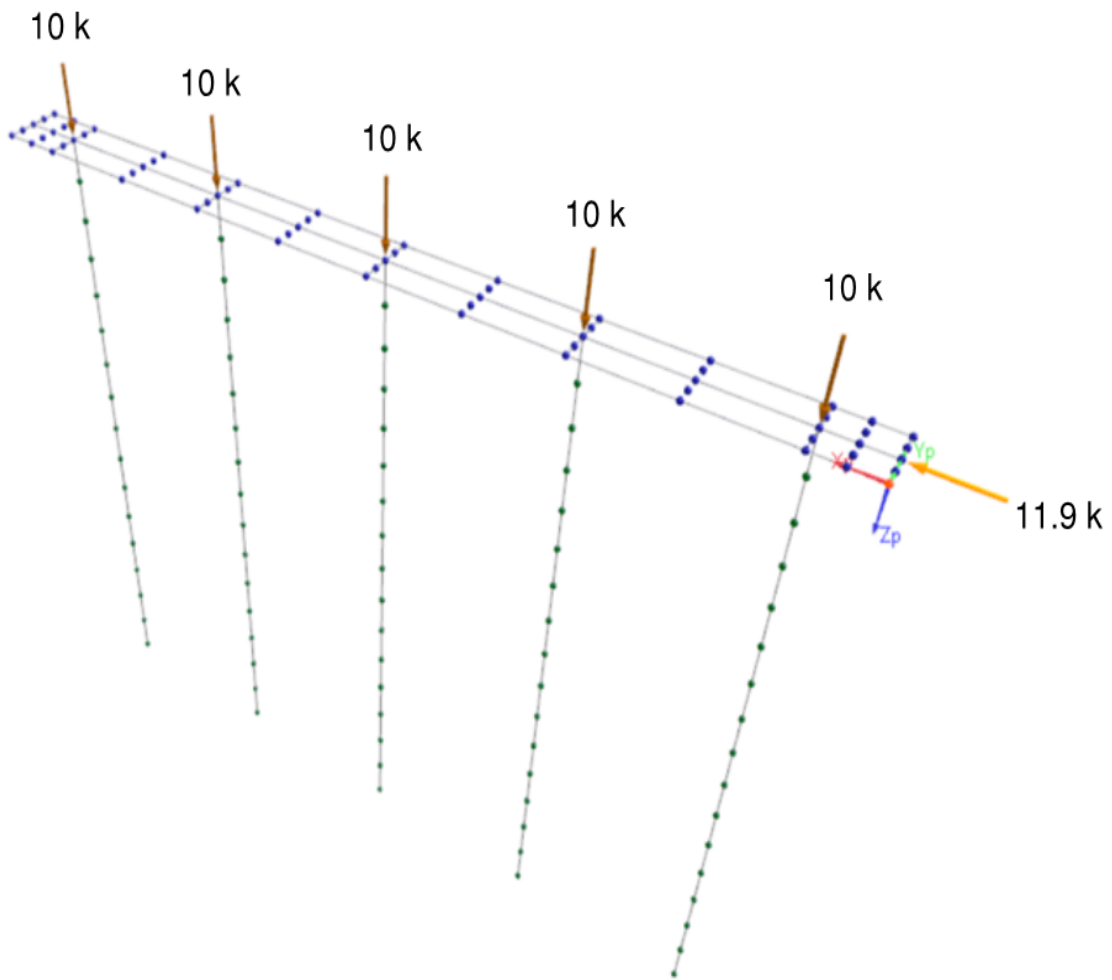


Figure 4.4 90% Single ply repaired damage at maximum load case.

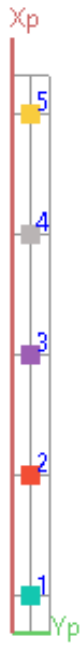


Figure 4.5 90% single ply repaired damage at maximum load case.

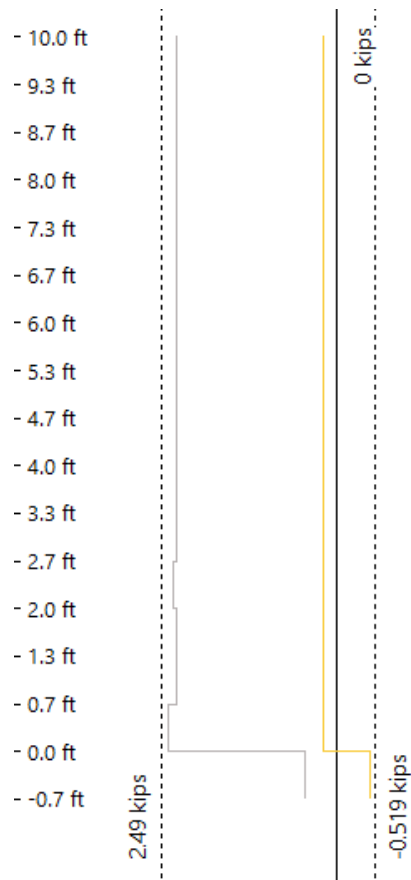


Figure 4.6 90% single ply repaired damage shear at maximum load case.

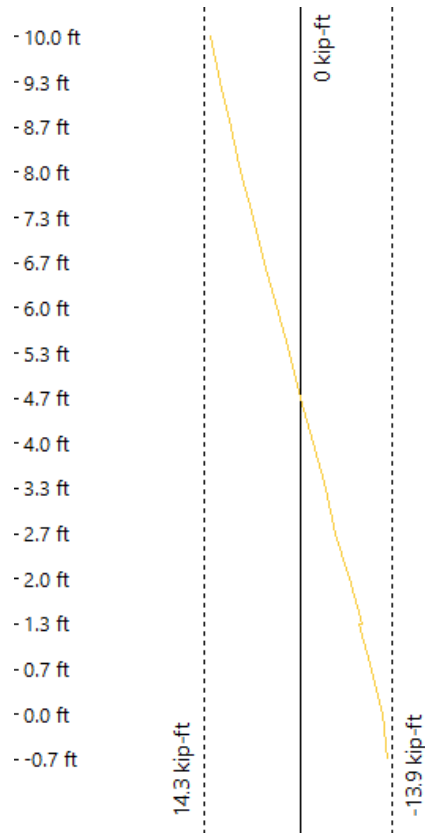


Figure 4.7 90% single ply repaired damage moment at maximum load case.

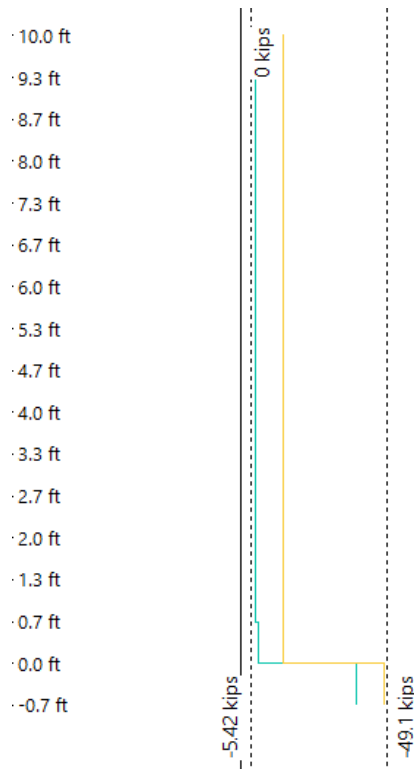


Figure 4.8 90% single ply repaired damage axial at maximum lateral loading.

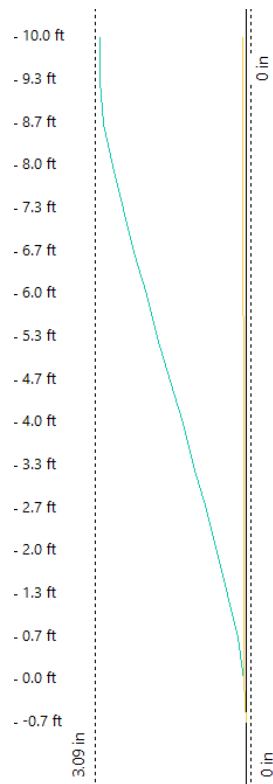


Figure 4.9 90% single ply repaired damage displacement at maximum load case.

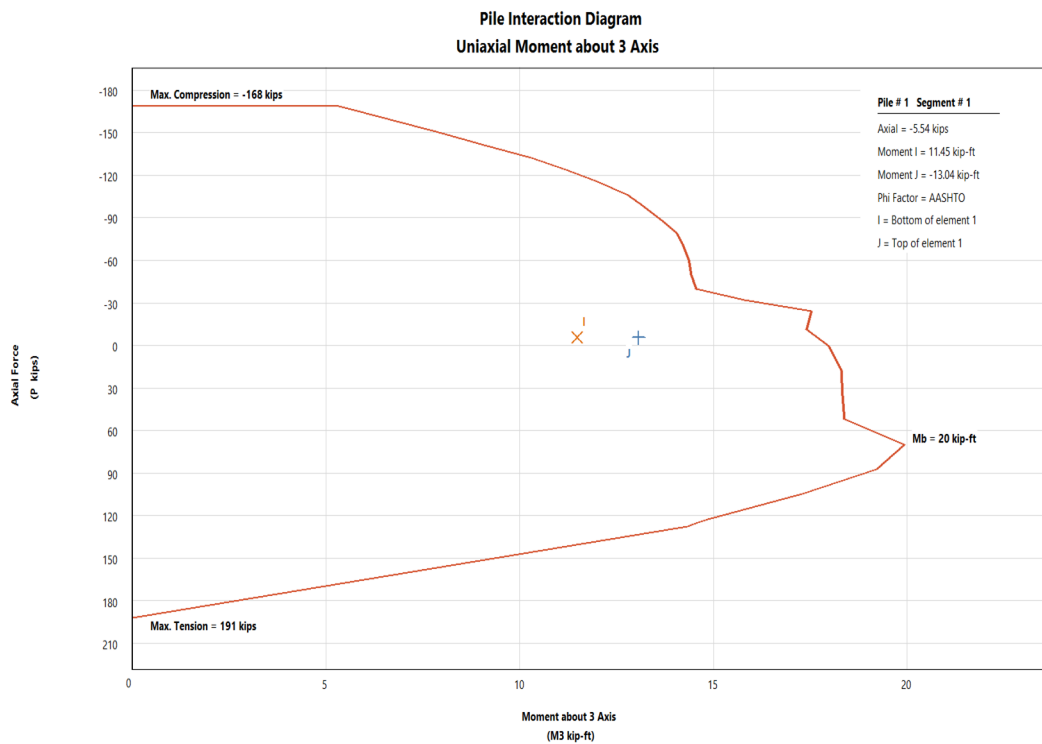


Figure 4.10 Interaction diagram single ply damage repaired at load case 10.

## CHAPTER 5: CONCLUSIONS

### 5.1 Study Summary

The objective of this experiment was to accurately model corrosion damage and the repair of corrosion damage to a third scale bridge bent using exteriorly applied carbon fiber properties with non-linear analysis. To do so, the utilization of test results from a previous study were considered in order to provide a reference undamaged control model to generate damaged and repaired damage models. Results indicated that in wrapping a pile with CFRP, pile stiffness within the elastic region minimally increases and plastic ductile capacity significantly increases.

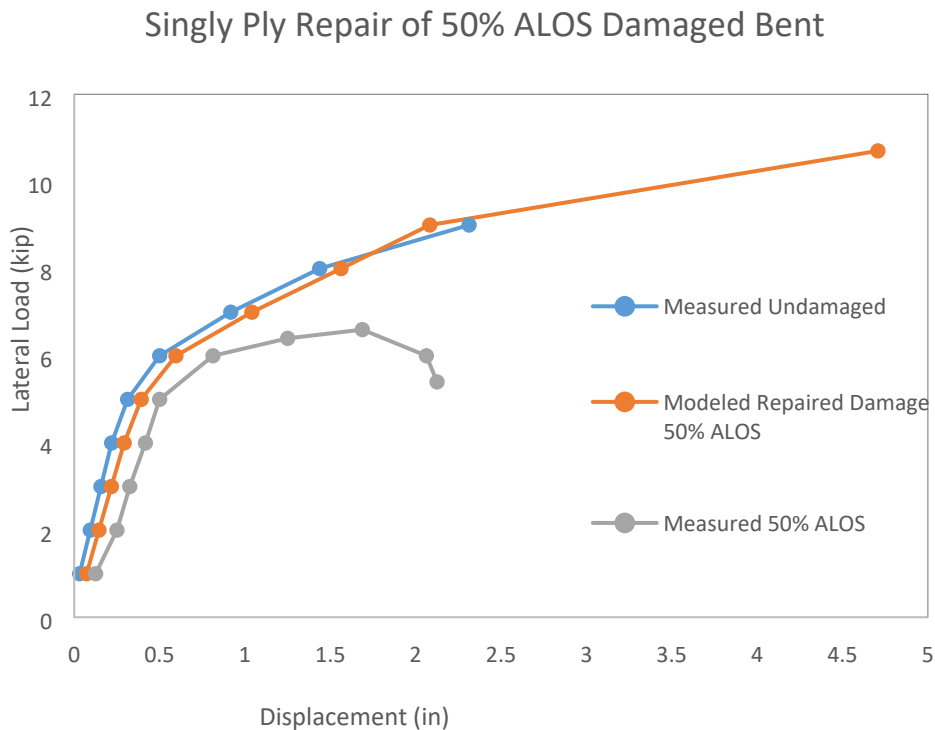


Figure 5.1 Response of measured, modeled and repaired at 50% damage.

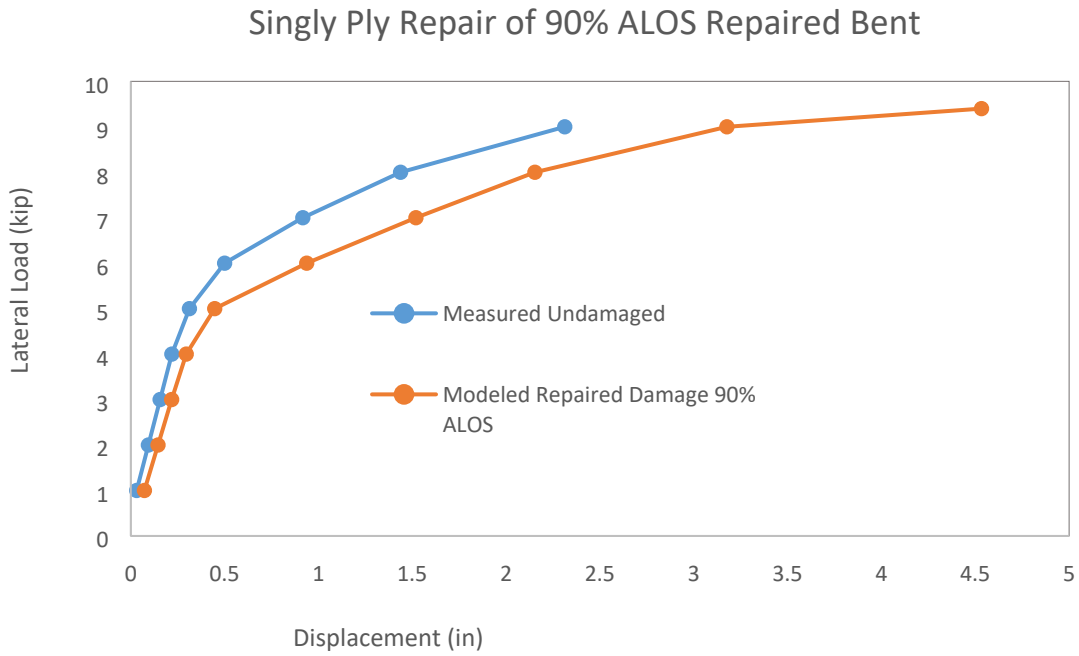


Figure 5.2 Measured damage vs single ply repair modeled damage at 90%.

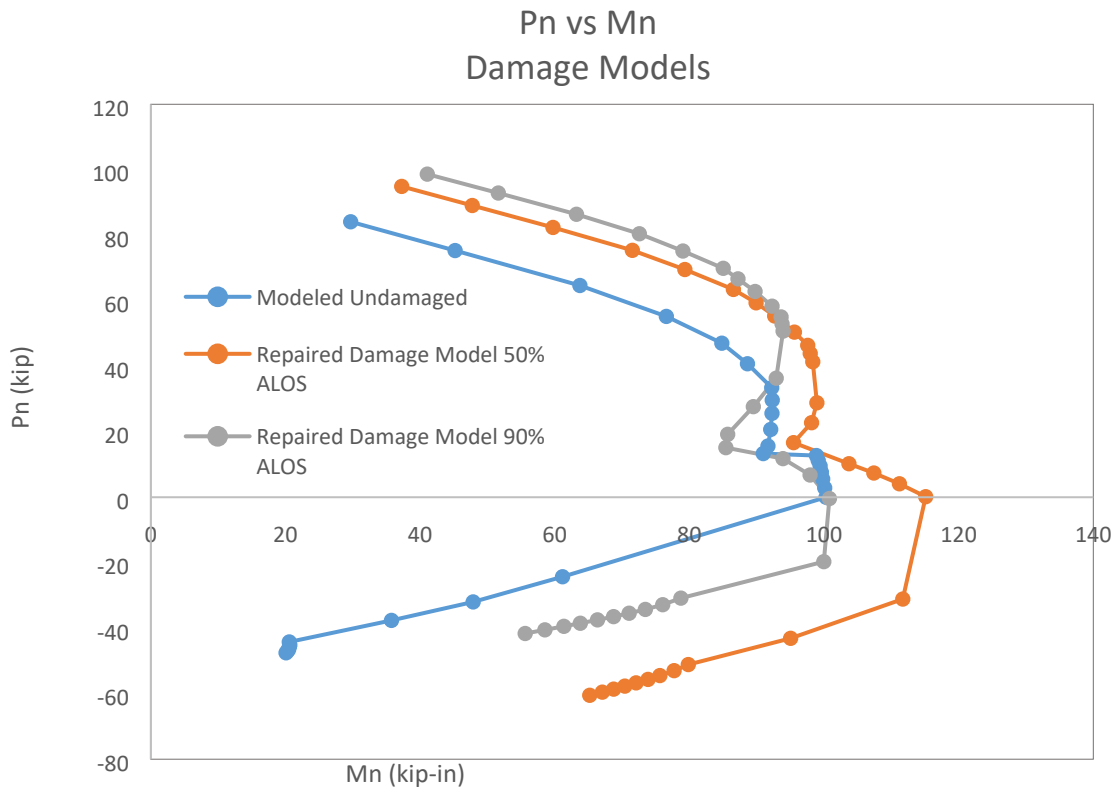


Figure 5.3 Interaction diagram of control model and repaired damage.

## **5.2 Interpretations of Findings**

The loss in ductility a bridge bent exhibits when it has succumb to damages by chloride induce corrosion is of concern to engineers when investigating the service life of an aged marine infrastructure. Although prestressing in the steel of a reinforced concrete member reduces as the area of steel reduces, what may be more concerning is the loss of a piles concrete cover, especially when loaded laterally. Modeling repaired damage to a bridge bent with FRP theoretically illustrated that a bridge bents bi-axial capacity increases considerably and provides more ductile behavior to a third scale experimental damaged bridge bent.

Predictive modeling of strength increase to a bridge bent repaired by FRP may lend usefulness in load rating damaged bridges and determine a means to restore or improve the integrity of marine infrastructure. In cases where emergency repairs are needed such as vessel collision to bridge piles, CFRP shows promise in restoring a piles capacity until more in depth investigations of damages are performed.

## **5.3 Future Work**

Future work involves the physical repair of the experimental bridge bent. This will include the construction of the bent cap and footer, FRP installment, erection of the bent, instrumentation, lateral load testing, data collection and analysis and cross examination between the actual testing results and the modeled results. Instrumentation and testing of CFRP material to determine bond effectiveness, actual chloride concentration levels within the contaminated region of the piles and gravimetric testing of actual loss in area of steel, would provide further understanding as to the efficacy of the models in replicating damage and repair of damage to a scaled bridge bent system.



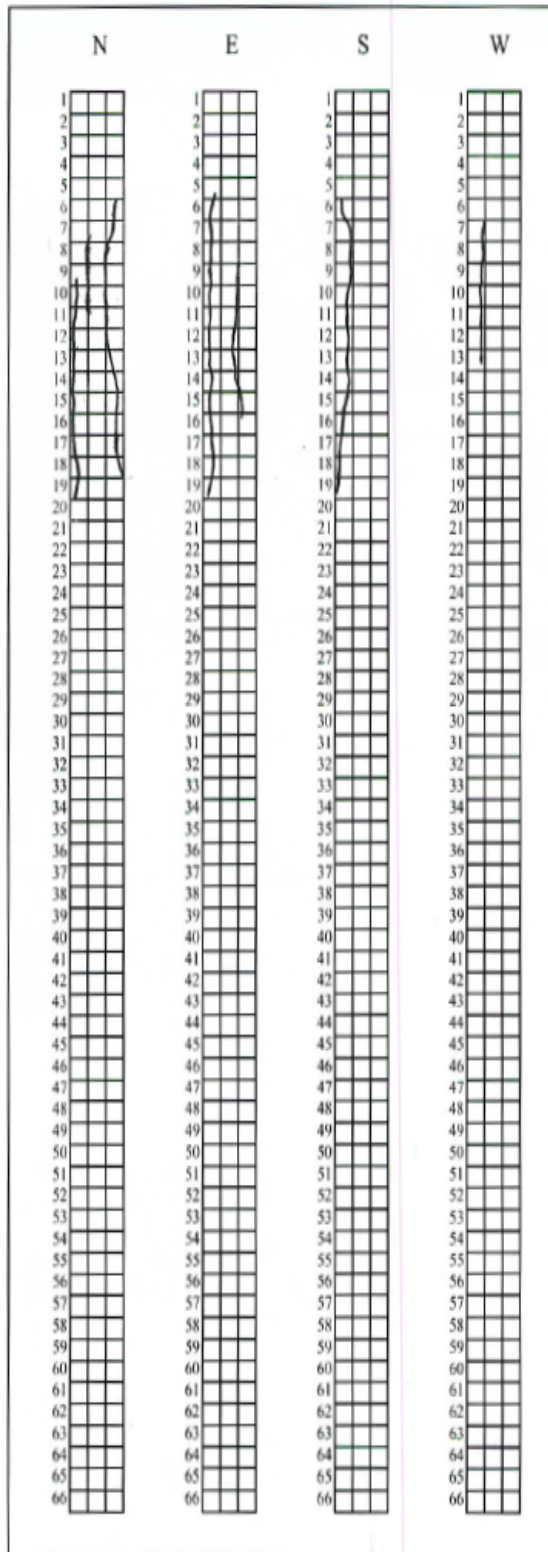
## REFERENCES

- American Association of State Highway and transportation Officials. (2012). *Guide Specifications for Design of Bonded FRP Systems for Repair and Strengthening of Concrete Bridge Elements*. Washington, DC.
- American Concrete Institute. (1989). *Corrosion of Metals in Concrete*. Detroit, MI.
- American Concrete Institute. (2002). Carbon Fiber-Reinforced Polymer Wraps for Corrosion Control and Rehabilitation of Reinforced Concrete Columns. *ACI Materials Journal*, 129-137.
- American Concrete Institute. (2008). *Guide for the Design and Construction of Externally Bonded FRP Systems for Strengthening Concrete Structures*. Farmington Hills, MI.
- American Concrete Institute. (2012). *Guide Test Methods for Fiber-Reinforced Polymer (FRP) Composites and Reinforcing or Strengthening Concrete and Masonry Structures*. Farmington Hills, MI.
- American Concrete Institute. (2013). *Code Requirements for Evaluation, Repair, and Rehabilitation of Concrete Buildings (ACI 562-13)*. Farmington Hills, MI.
- American Concrete Institute. (2014). *Building Code Requirements for structural Concrete (ACI 318-14) and Commentary on Building Code Requirements for Structural Concrete (ACI 318R-14)*. Farmington Hills, MI.
- Goulish, A. (2002). *Lateral Capacity of Corrosion Damaged Pile Bents*.
- Hibbeler, R. C. (2012). *Structural Analysis* (8 ed.). Pearson Prentice Hall.
- Mullins, G. A., Sen, R., & Goulish, A. J. (2002, May). Lateral Capacity of Corrosion Damaged Pile Bents. Tampa, FL.
- Mullins, G., Sen, R., Suh, K. S., & Winters, D. (2004). *Underwater FRP Pile Wrap of the Friendship Trails Bridge*. Tampa, FL: University of South Florida.
- Mullins, G., Sen, R., Suh, K., & Winters, D. (2005). Underwater Fiber-Reinforced Polymers Repair of Prestressed Piles in the Allen Creek Bridge. *Journal of Composites for Construction*, 136-146.
- Nawy, E. G. (2001). *High-Performance Concrete* (2 ed.). John Wiley & Sons, Inc.
- Wight, J. K. (2016). *Reinforced Concrete Mechanics and Design* (7 ed.). Pearson and Prentice Hall.

Winters, D., Mullins, G., Sen, R., Schrader, A., & Stokes, M. (2008). Bond Enhancement for FRP Repair in Tidal Waters. *Journal of Composites for Construction*, 334-343.

## **APPENDIX A: PILE DEFICIENCY MAPPING**

FEB-1-17



Pile: S223

North Face:

Number of Cracks: 3

Mean Length: 21" 5" 26"

Max Width: 1/8" 1/32" 1/16"  
                  1      2      3

East Face:

Number of Cracks: 2

Mean Length: 23" 16"

Max Width: 1/16" 1/32"

South Face:

Number of Cracks: 1

Mean Length: 27"

Max Width: 1/16"

West Face:

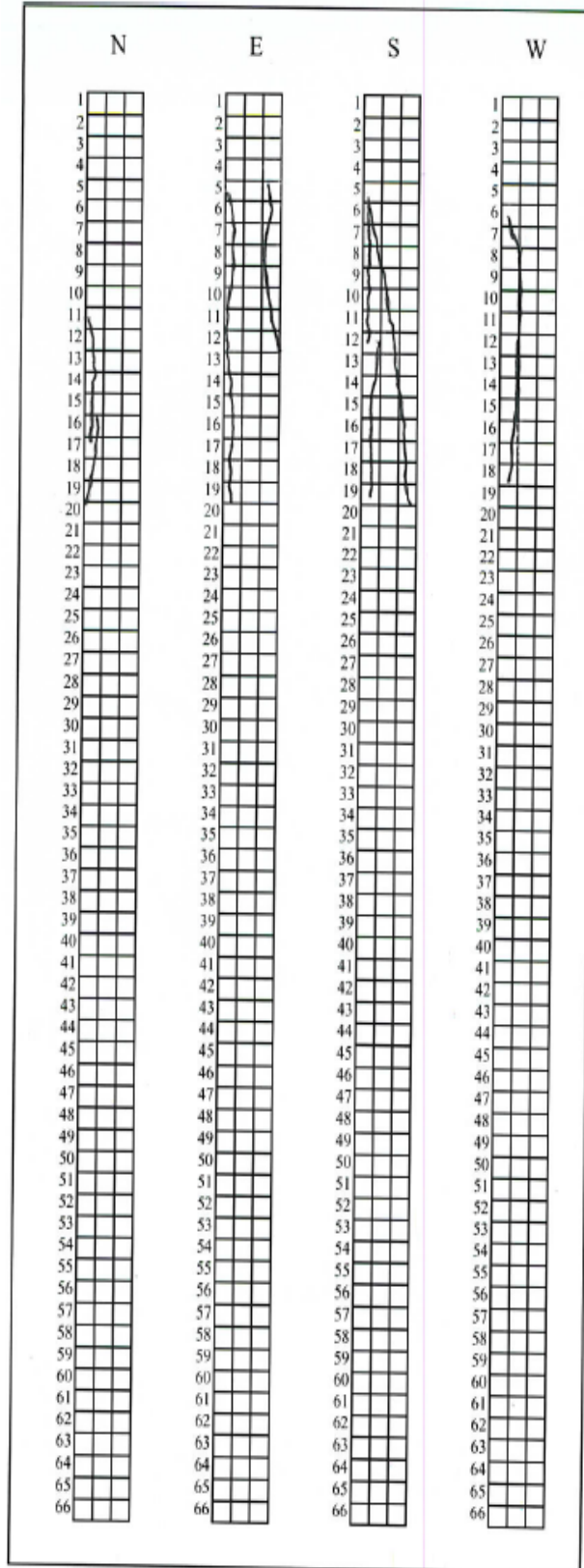
Number of Cracks: 1

Mean Length: 15"

Max Width: 1/32"

Notes:

Figure A.1 Pile S223 deficiency map.



Pile: S222

North Face:

Number of Cracks: 2

Mean Length: 9" 12"

Max Width: 1/8" 1/16"

East Face:

Number of Cracks: 2

Mean Length: 29" 15"

Max Width: 1/16" 1/8"

South Face:

Number of Cracks: 3

Mean Length: 10" 27" 16"

Max Width: 1/32" 1/32" 1/32"  
 (1) (2)

West Face:

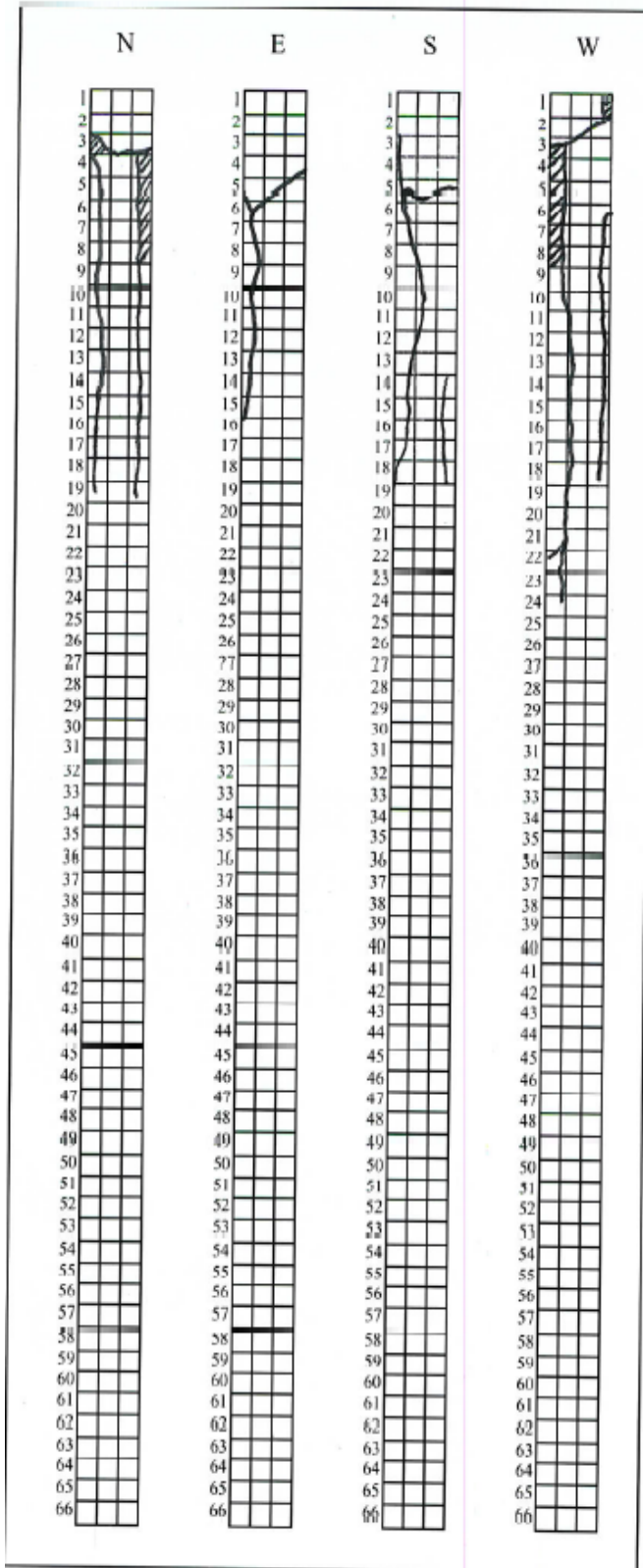
Number of Cracks: 1

Mean Length: 27"

Max Width: 1/16"

Notes:

Figure A.2 Pile S222 deficiency map.



Pile: S221

North Face:

Number of Cracks: 2

Mean Length: 34" 34"

Max Width: 1/2" 1/4"

East Face:

Number of Cracks: 1

Mean Length: 24"

Max Width: 1/4"

South Face:

Number of Cracks: 2

Mean Length: 34" 10"

Max Width: 1/8" 1/16"

West Face:

Number of Cracks: 2

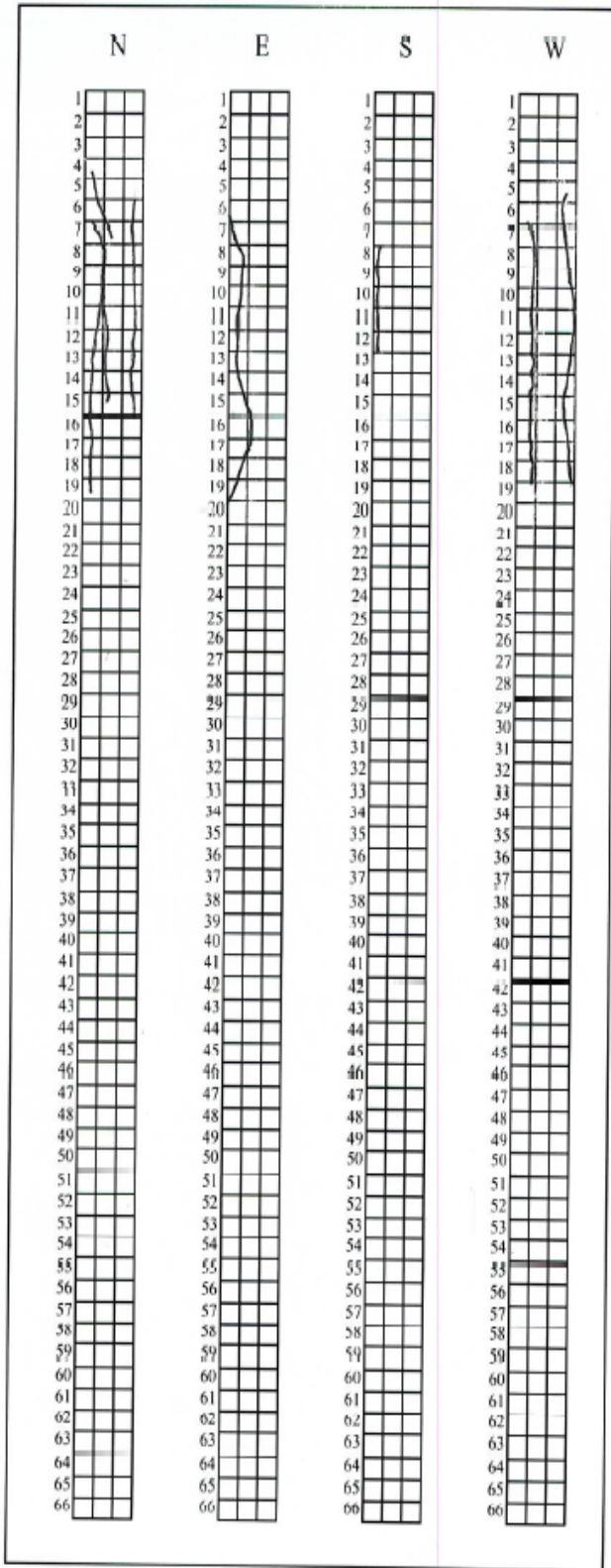
Mean Length: 48"

Max Width: 1/2" = 3/4"

Notes:

SEPARATION OF COVER  
EAST FACE  
NORTH FACE  
SOUTH FACE

Figure A.3 Pile S221 deficiency map.



Pile: S220

North Face:

Number of Cracks: 3

Mean Length: 25" 7" 19"

Max Width: 1/16" 1/32" 1/32"

East Face:

Number of Cracks: 1

Mean Length: 30"

Max Width: 1/16"

South Face:

Number of Cracks: 1

Mean Length: 12"

Max Width: 1/16"

West Face:

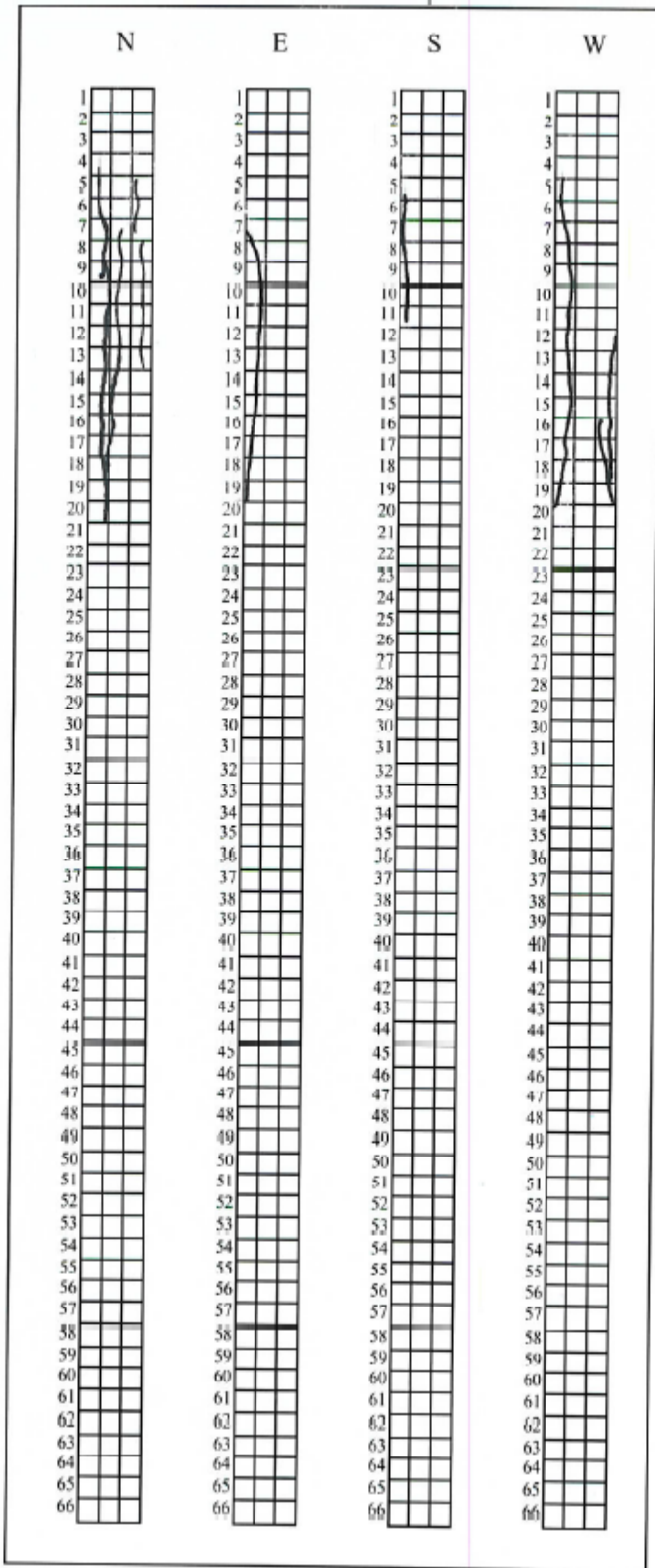
Number of Cracks: 2

Mean Length: 24" 27"

Max Width: 1/16" 1/32"

Notes:

Figure A.4 S220 deficiency map.



Pile: S218

North Face:

Number of Cracks: 3

Mean Length: 33" 29" 13"

Max Width: 1/4" 1/32" 1/32"  
③

East Face:

Number of Cracks: 1

Mean Length: 24"

Max Width: 1/8"

South Face:

Number of Cracks: 1

Mean Length: 4"

Max Width: 1/8"

West Face:

Number of Cracks: 2

Mean Length: 30" 14"

Max Width: 1/8"

Notes:

Figure A.5 S218 deficiency map.



## **APPENDIX B: OUTPUT RESULTS GRAPHS**

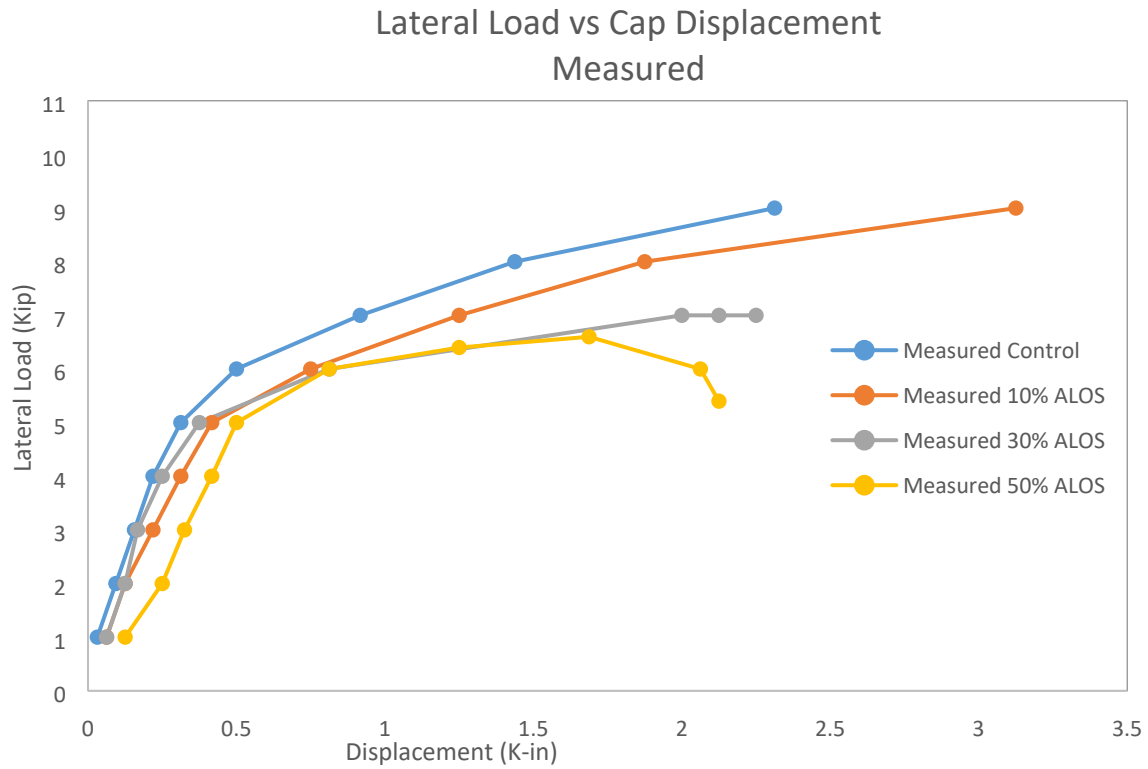


Figure B.1 Measured test data from undamaged pile bent.

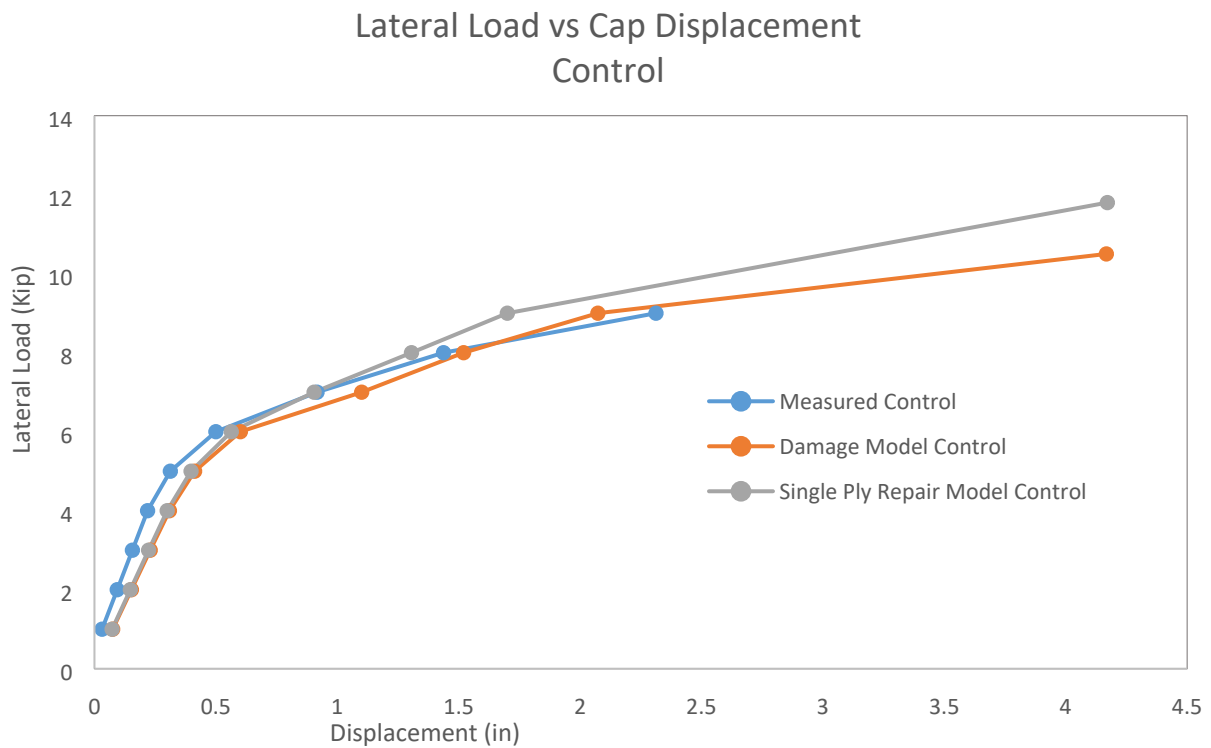


Figure B.2 Undamaged model, undamaged measured model, undamaged repaired model.

### Lateral Load vs Cap Displacement 10% Area Loss of Steel

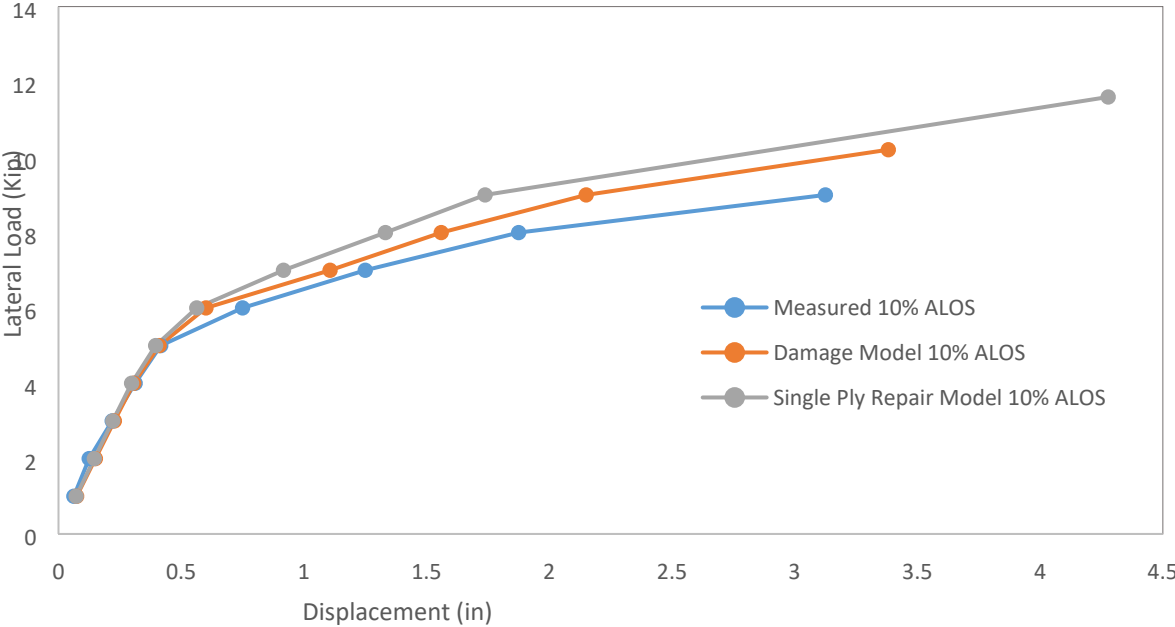


Figure B.3 10% Damage model, 10% measured damage, 10% repaired damage.

### Lateral Load vs Cap Displacement 30% Area Loss of Steel

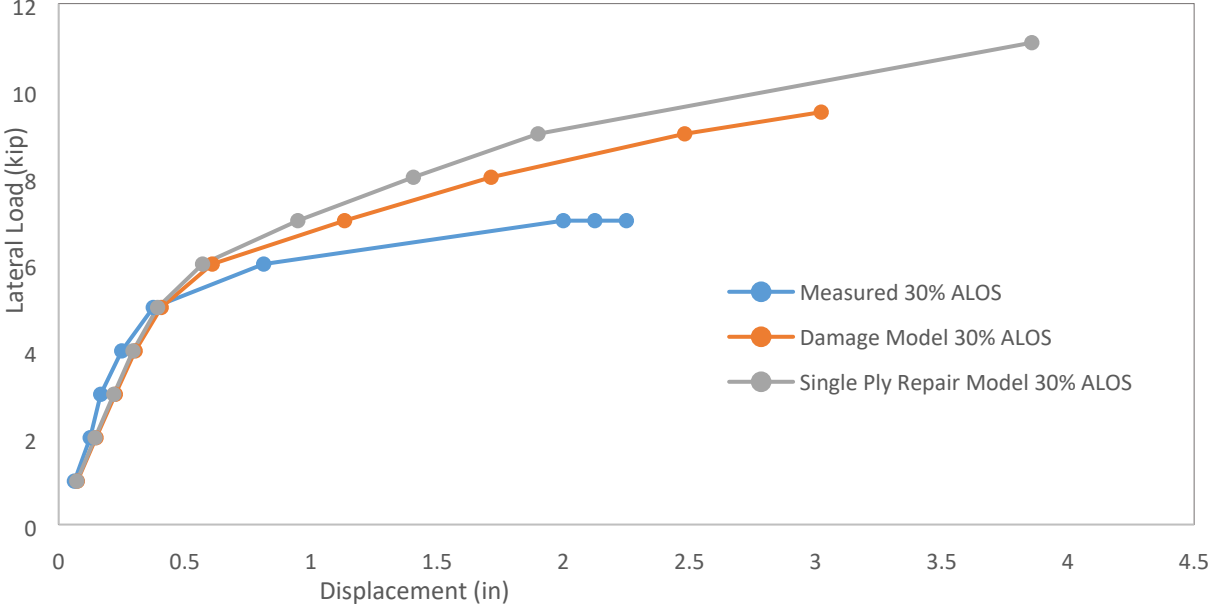


Figure B.4 30% Damage model, 30% measured damage, 30% repaired damage.

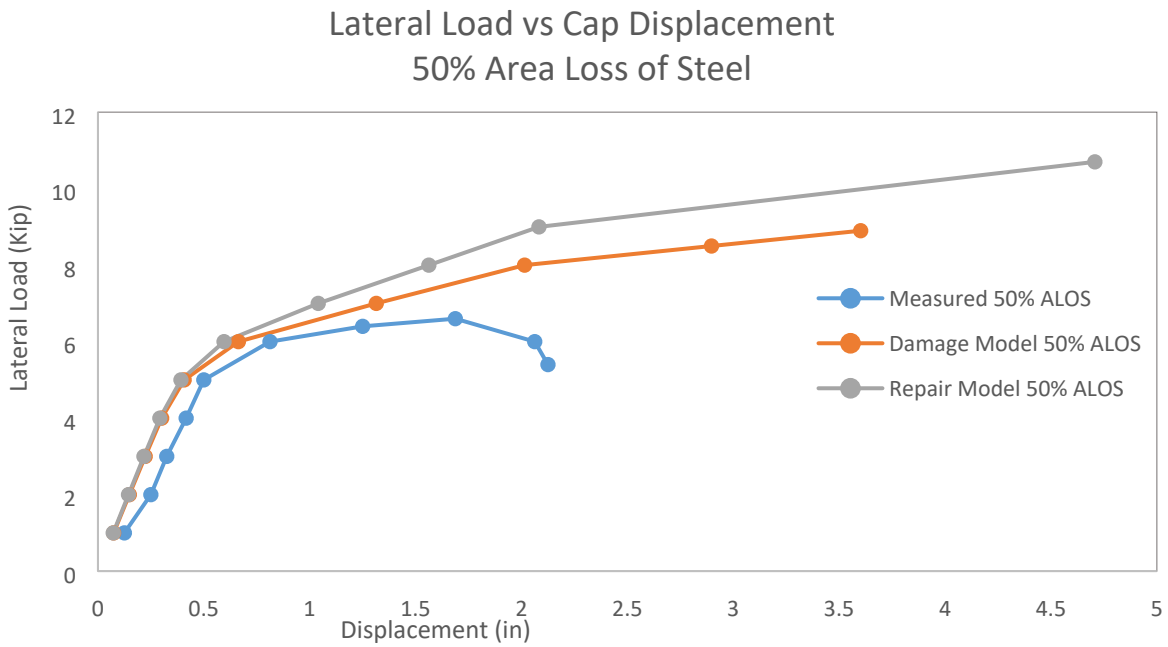


Figure B.5 50% Damage model, 50% measured damage, 50% repaired damage.

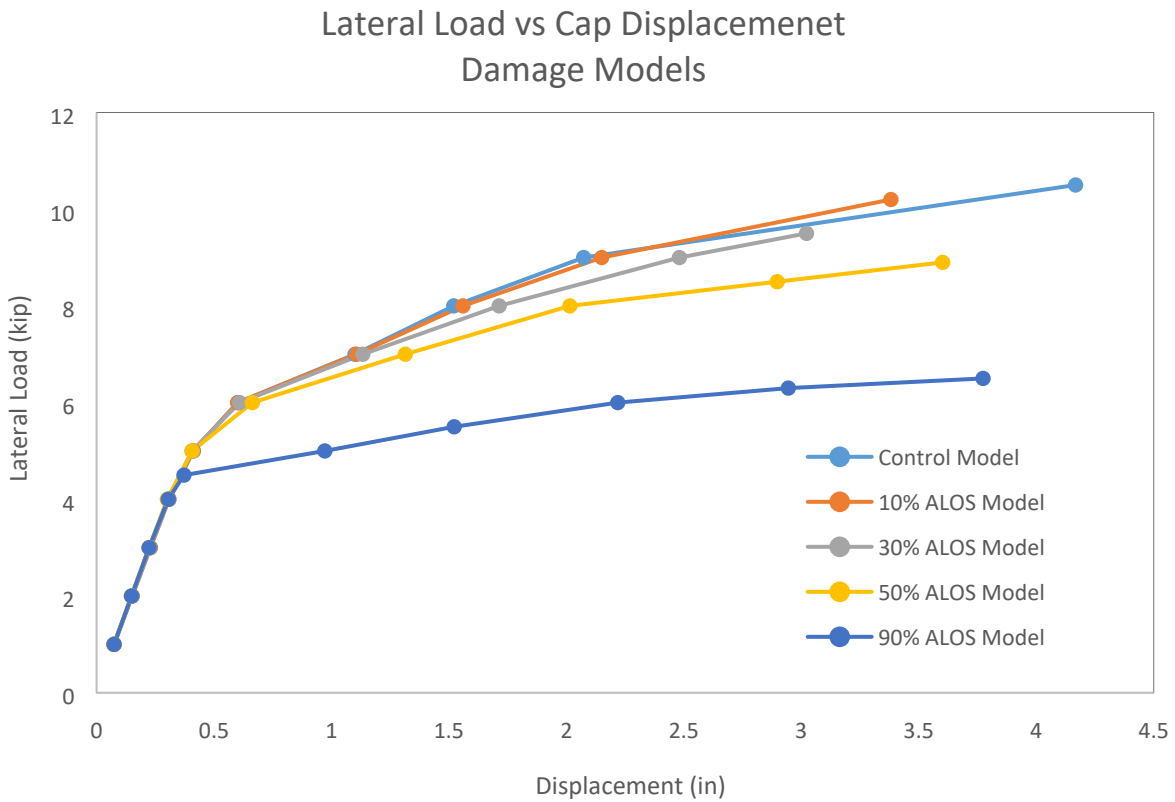


Figure B.6 All damaged models.

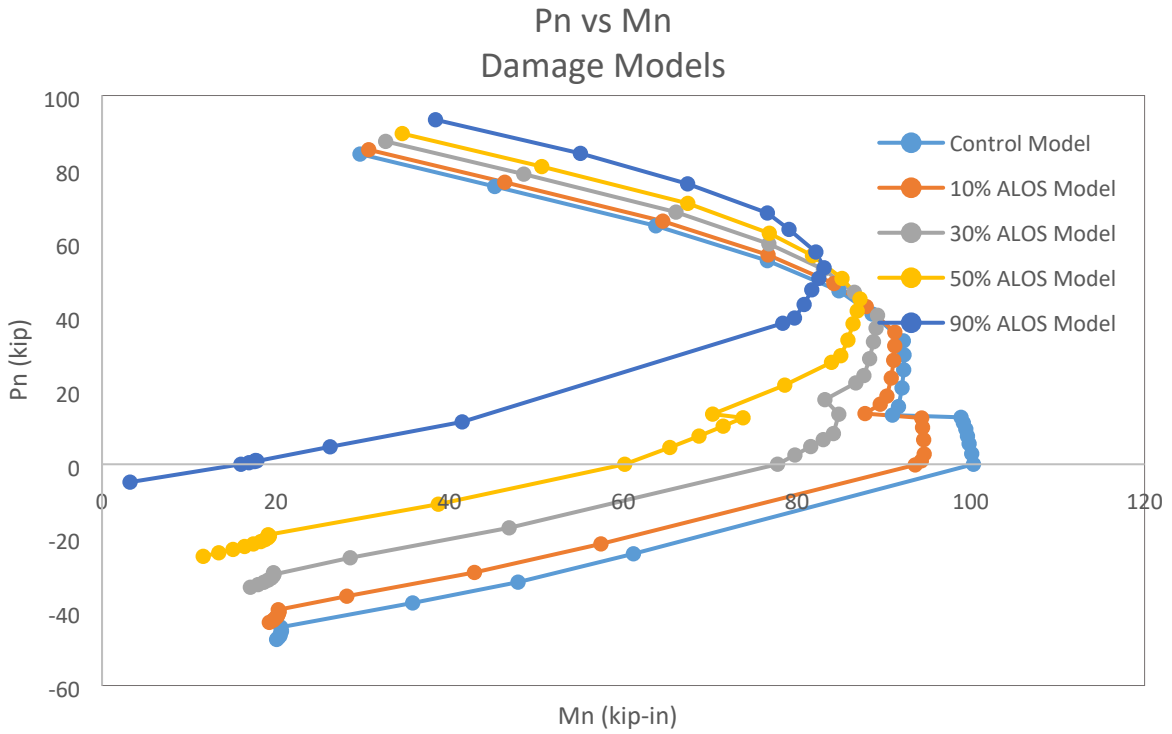


Figure B.7 Interaction diagram of all damaged models.

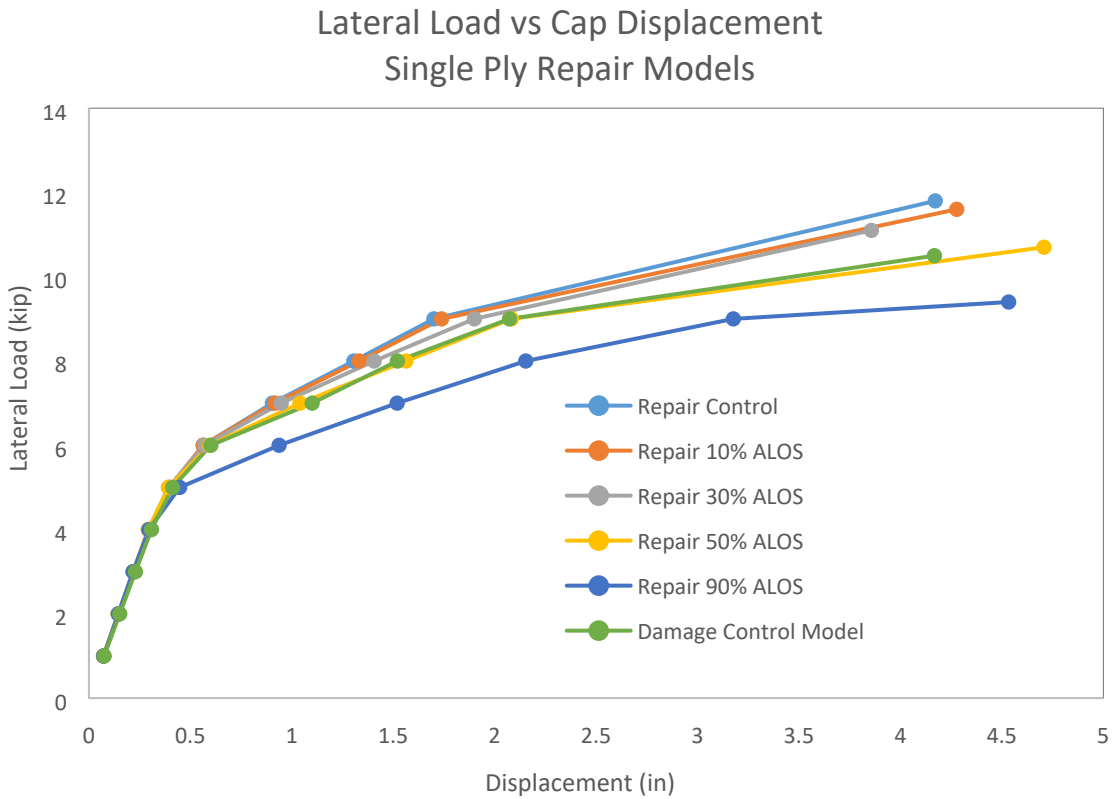


Figure B.8 Lateral load response for all repaired damage models.

### Pn vs Mn Single Ply Repair Models

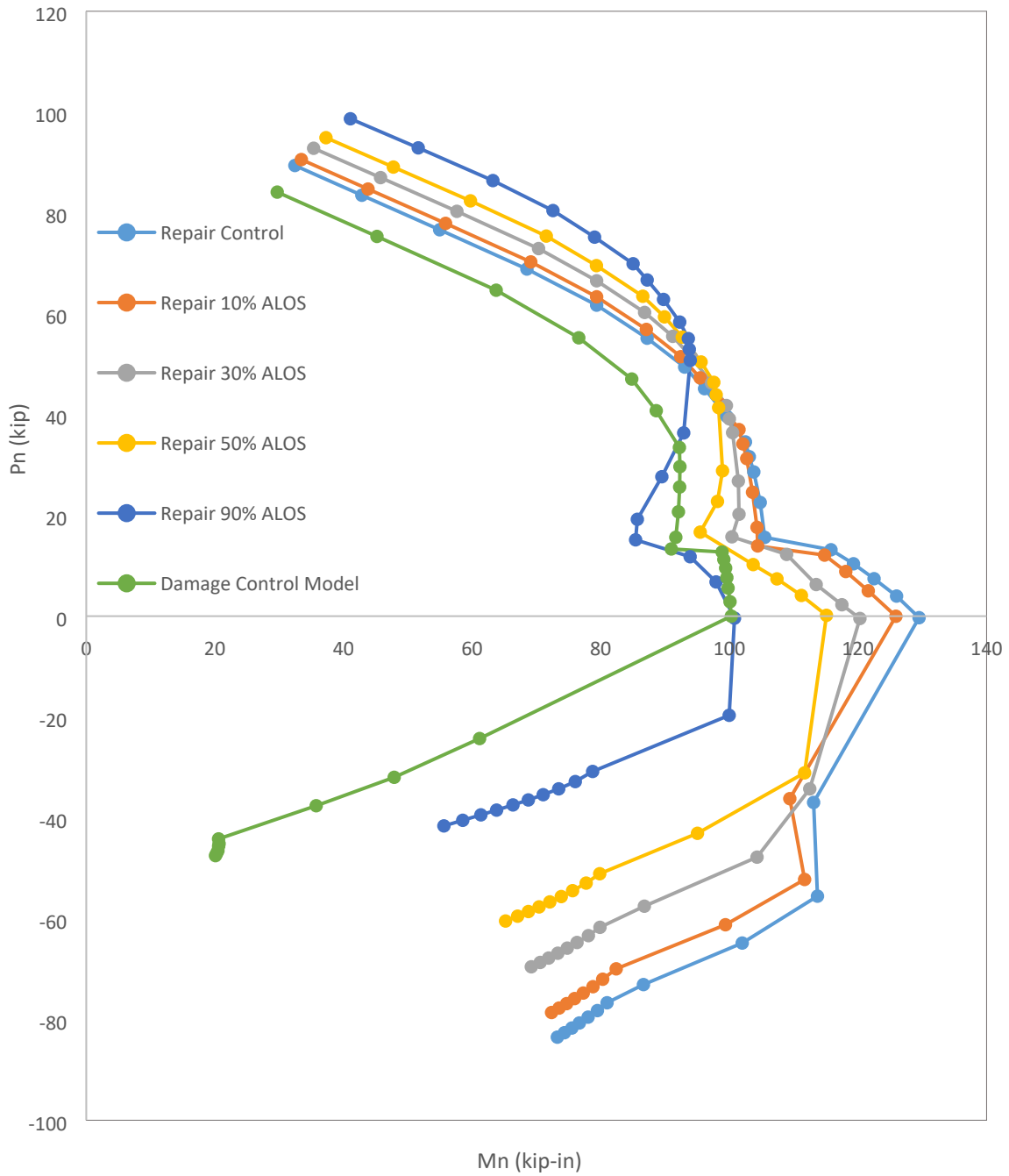


Figure B.9 Interaction diagram envelope for all repaired damage models.